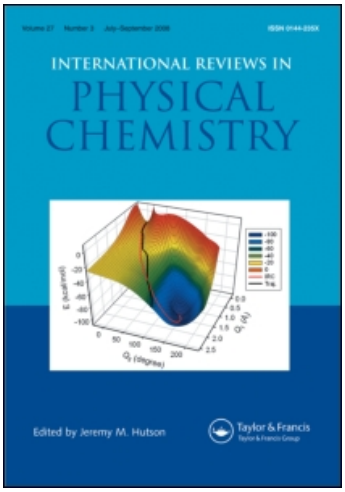

International Reviews in Physical Chemistry
Publication details, including instructions for authors and subscription information:
http://www.informaworld.com/smpp/title~content=t713724383

Rotational Fine Structure in Dynamic Photophysical Processes

E. W. Schlag[a]; W. E. Henke[a]; S. H. Lin[b]
[a] Institute for Physical and Theoretical Chemistry, Technical University of Munich, Garching, West Germany [b] Department of Chemistry, Arizona State University, Tempe, AZ, USA

To cite this Article Schlag, E. W. , Henke, W. E. and Lin, S. H.(1982) 'Rotational Fine Structure in Dynamic Photophysical Processes', International Reviews in Physical Chemistry, 2: 1, 43 — 94
To link to this Article: DOI: 10.1080/01442358209353328
URL: http://dx.doi.org/10.1080/01442358209353328

International Reviews in Physical Chemistry (1982), *2* (43–94)

ROTATIONAL FINE STRUCTURE IN DYNAMIC PHOTOPHYSICAL PROCESSES

E. W. SCHLAG, W. E. HENKE

Institute for Physical and Theoretical Chemistry, Technical University of Munich, 8046 Garching, West Germany

AND

S. H. LIN

Department of Chemistry, Arizona State University, Tempe, AZ 85281, USA

ABSTRACT

Experimental and theoretical results of the photophysics of single rovibronic states are reviewed. Particular emphasis is placed on the dependence of the non-radiative rate constant on the excited rotational state. In contrast to previous pessimism it is shown that the experimentally determined range in single rovibronic level lifetimes can be theoretically rationalized. Quantum beats in the fluorescence decay of single rotational states are also included. Important information about dephasing, build-up and decay of initially excited quantum states and their coupling with the other excited electronic state can thus be obtained.

INTRODUCTION

A transition between two electronic states can be radiative or non-radiative. Radiative transitions are well known to depend on the electronic, vibrational and rotational state. However, the situation is not so clear for non-radiative transitions although they have been the subject of many recent studies by molecular physicists, chemists and photobiologists. Experimentalists were first able to measure the canonical rate constants in the liquid and solid phase, i.e. the rate constants averaged by the Boltzmann factor over the rotational vibrational states in the exited electronic manifold under consideration (Robinson and Frosch, 1962; Jortner *et al.*, 1969; Schlag *et al.*, 1971; Robinson, 1974; Henry and Siebrand, 1973). It was shown that the transition rate depends on the electronic energy gap or the amount of vibrational energy in the final state. Later collisionless experiments were performed where individual vibrational states could be probed (Freed, 1976; Avouris *et al.*, 1977). The lifetime was found to depend on the vibrational state due to Franck–Condon weighted density of states overlap factors. So far the constraints of conservation of total energy and linear momentum were considered. But in addition all physical processes are governed by the conservation of angular momentum. Thus the next question was to ask if there is a rotational dependence of the radiationless transition rate. From the experimental side this required probing of single rotational states which became feasible with recent

improvement in laser, molecular beam and hypersonic jet technology. With the stimulus from the experimental findings, the theory of photophysical processes has been developed accordingly.

This review is concerned with the experimental and theoretical aspects of the participation of molecular rotational states in photophysical processes. Several reviews related to this subject have appeared recently (Lee, 1977; Lee and Loper, 1980; Howard and Schlag, 1980; Novak *et al.*, 1980). Thus this review is restricted to the more recent experimental and theoretical results. Because of the limited space available, an exhaustive review of this subject is not attempted and only a number of representative cases will be considered.

EXPERIMENTAL STUDIES

Up to 1979 there were only a few studies concerned with the fate of single rovibronic levels in polyatomic molecules. This is mainly due to fast collisional rotational relaxation which spreads a narrow initial excitation to a broad distribution of other rotational states. Because of this rapid rotational relaxation it was necessary to carry out the experiments at lower and lower 'zero pressure' regimes.

Another factor is that the exciting light must be sufficiently narrow and the lines non-overlapped so that a single rovibronic state can be excited. For large molecules the rotational lines lie within the Doppler-width. Either Doppler-free methods have to be used or other methods which allow differentiation between the simultaneously excited rotational levels such as measurements of resolved fluorescence have to be employed. Such techniques were not feasible when the first investigations on rotational state dependence were performed. Many rotational levels were excited simultaneously by a broad-band laser in these early experiments. The laser was then tuned across the rotational contours and any change in lifetime or quantum yield was related to the excited state rotational distribution. The results obtained in this way are always averaged over many rotational states and are thus not as useful as single rovibronic level measurements. In the following therefore the broad-band studies are only briefly mentioned and the available single rotational level measurements are reported in detail.

Broadband rotational measurements

Parmenter and Schuh (1972) investigated the rotational state dependence in benzene and reported a negative result. The fluorescence quantum yields were measured along the rotational contours of several vibronic bands of the benzene $S_1 \leftarrow S_0$ transition. To within the stated accuracy of 10% no dependence of the yield on initially excited rotational levels was found. However, as Coveleskie and Parmenter (1978) point out, rotational relaxation cannot be excluded. They state that no strong selection rules seem to apply and that at the pressures used in the investigation (0.1 Torr) 40% of the molecules undergo rotational state changes before non-radiative decay. The wide distribution of levels so created seriously damps the sensitivity of these experiments in detecting rotational effects.

Measurements by Boesl *et al.* (1975) revealed structure in the lifetime spectrum while tuning across the electronic origin of naphthalene. Maxima in lifetime occurred at the same positions as maxima in absorption. Howard and Schlag (1978a) measured quantum yields along the rotational contour of naphthalene which indicated a dependence on the excited rotational state distribution. Both naphthalene experiments were carried out at 0.07 Torr. At this pressure Coveleskie and Parmenter (1978)

calculate that 65% of the S_1 molecules will undergo collisions which change rotational state, if the rotational relaxation rate for benzene is used. Possibly, the cross-section is smaller, or possibly stronger selection rules exist for $\Delta J'$, $\Delta K'$ changes so that while collisions change rotational states, they do not initially create severe disturbances of rotational distributions.

All these experiments had the disadvantage that many rotational states were probed simultaneously, which decreased the sensitivity of detecting rotational effects.

Single rovibronic measurements

In this section a review of measurements of single rotational state lifetimes and quantum yields will be attempted. Diatomic and triatomic molecules have been excluded since they very often predissociate directly after optical excitation and this mechanism will not be discussed. Internal conversion and intersystem crossing are reported. Molecules like formaldehyde which dissociate after excitation are included, however, since the initial decay of the excited state is believed to be internal conversion and can thus be treated by the models discussed in the section on theory.

Glyoxal

Parmenter and Rordorf (1978) measured single rotational quantum yields in the vibrationless electronically excited (^1A_u) state of glyoxal. A narrow band argon ion laser was used to excite several rotational states collectively, the average spacing between rotational lines being smaller than the Doppler width. The fluorescence was dispersed and thus it was possible to study the relative contribution to the emission of each individual rotational state. This is a neat experiment since rotational relaxation can easily be shown to be absent if only those rotational states emit which are directly excited by the laser radiation. The quantum yields for five rotational levels are shown in *Table 1*. They vary by more than 20%. It is not clear if this variation can be totally

TABLE 1. Quantum yields and lifetimes of single rovibronic levels of the vibrationless electronically excited ^1A_u state of glyoxal*

J'	K'	E_{rot} (cm^{-1})	Φ (arb. units)	τ (μs)
18	5	139.93	0.93	2.29
46	5			
13	6			2.34 ($\pm$0.07)
12	6	88.60	1.04	
14	8		1.13	
46	5		0.93	
48	5	368.34		
18	5			
46	5			2.27
49	8			
49	8			2.31
12	6			
49	8			
12	6			2.24
25	8			

* Data from Parmenter and Rordorf (1978) and Michel and Tramer (1979).

attributed to experimental uncertainty or is in fact a rotational effect. The range in rotational energy which is probed is large and very different J' quantum numbers were measured, but only $K' = 5$ to 8 levels were examined. The rotational effect on quantum yield thus does not appear to be large in glyoxal but more systematic measurements for a wider variety of rotational states are needed.

Single rotational level lifetimes were reported by Michel and Tramer (1979) for glyoxal and are also shown in *Table 1*. Because of low signal intensities the fluorescence could not be resolved rotationally which resulted in a simultaneous lifetime measurement of several rotational states except for the $J' = 13$, $K' = 6$ rotational level. Only if the lifetimes of simultaneously measured levels differ significantly will then a biexponential decay be observed. As the decays were exponential, one can conclude from this and the small variation of lifetimes that the rotational effect on lifetimes in glyoxal must be small (~10–20%).

The effect of rotational state on collision induced intersystem crossing (CIISC) was investigated in a hypersonic jet by Jouvet and Soep (1980). They found that CIISC is insensitive to the initially excited rovibronic S_1 level with the exception of the $J' = 4$, $K' = 1$ level for which efficient CIISC was reported.

Pyrazine

Lifetime measurements on pyrazine in a hypersonic jet, were reported by Ter Horst *et al.* (1981). Single rotational excitation was not achieved, but in the R branch of the vibrationless ${}^1B_{3u} \leftarrow {}^1A_g$ transition which can be seen in *Figure 1* the $\Delta K = 0$ transitions overlap for each different J quantum number. So it is possible to excite individual J, but grouped K levels (K stacks). The plots of fluorescence decay versus time (*Figure 33*) are strongly biexponential for large J', due to an increase of decay rate with the square of the K quantum number. The smooth line in *Figure 33* is a theoretical fit to the experimental data and will be discussed in the section devoted to theory.

Quantum yields averaged over many rotational levels were investigated by Baba *et al.* (1980). They are shown in *Figure 2*. It can be seen that the yield increases rapidly at the high energy side of the Q branch. The transition energies for the Q branch are $\nu_Q = \nu_0 - 0.00126\ (J + J^2) - 0.0001 K^2$, so that the low rotational quantum numbers lie on the high energy side. Baba *et al.* (1980) propose that S–T coupling in pyrazine is enhanced by increasing rotation.

From spectroscopic studies of Innes *et al.* (1972) it is known that pyrazine has a large positive inertial defect $\delta' = I_c^0 - I_a^0 - I_b^0$ in its ${}^1B_{3u}$ excited state. Negative inertial defects can result from deviations from molecular planarity. However, positive defects are very unusual and are tentatively attributed by Innes *et al.* (1972) to a mixing of the ${}^1B_{3u}$ state with a perturbing electronic state, that is, to deviations from the Born–Oppenheimer approximation, which may be due to electronic Coriolis interaction. Very recently Ohta and Baba (1981) observed rotational effects on the quantum yield and lifetime in the fluorescence from *s*-triazine.

Formaldehyde

The peculiarity of the formaldehyde problem has intrigued physical chemists for many years. Formaldehyde has been called the prototype for the photochemistry of small polyatomics but many important questions concerning the photochemical mechanism still remained unanswered. In recent years, formaldehyde has developed into the probing ground for theories of non-radiative (NR) decay. One may claim that it is the best-studied molecule, its spectroscopy and chemical decay being well-documented. An

enormous amount of prerequisite information about singlet–triplet perturbation (Kusch and Loomis, 1939; Stevens and Brand, 1973; Brand and Stevens, 1973; Brand and Liu, 1974; Birss *et al.*, 1978; Barnett *et al.*, 1979; Ramsay and Till, 1979), Coriolis coupling (Parkin *et al.*, 1962; Tanaka *et al.*, 1975), Fermi resonance (Sethuraman *et al.*, 1970) and predissociation is already available from high-resolution optical spectroscopy. All this led to the belief that it is the ideal system to investigate the rotational state dependence of the NR rate constants.

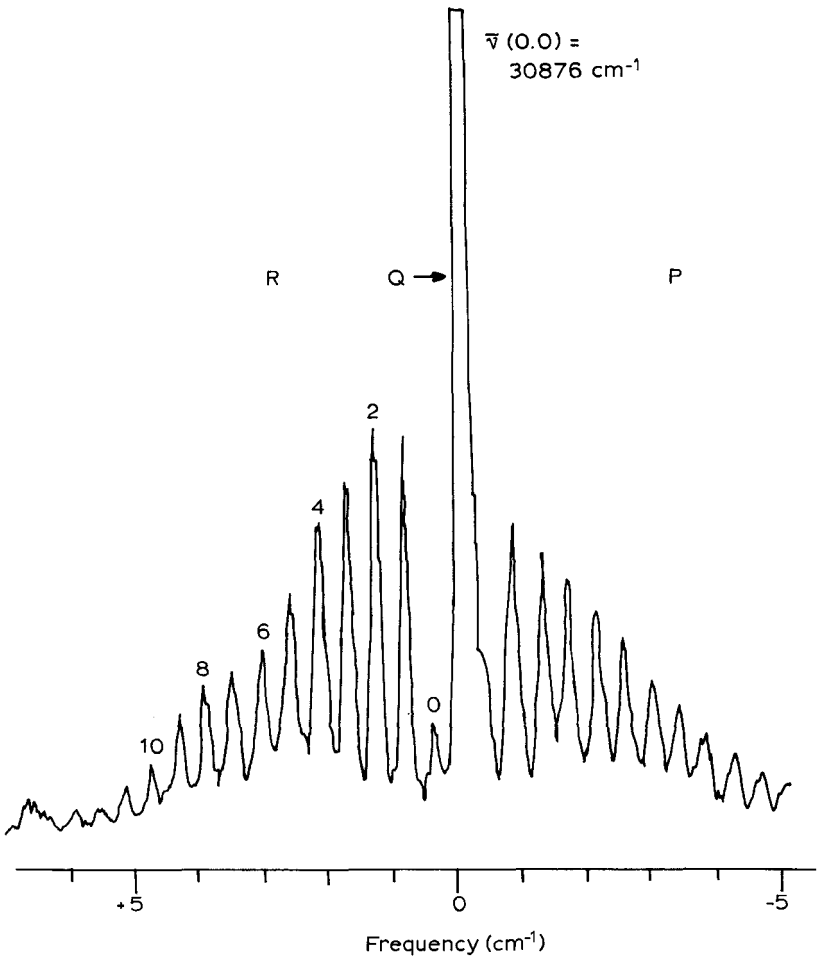

FIG. 1. Fluorescence excitation spectrum of the (0,0) C-type band of the $^1B_{3u} \leftarrow {}^1A_g$ transition of pyrazine-h_4. The ground state values J'' of lines containing all the $\Delta K = 0$ transitions with $K \leqslant J''$ are indicated in the R branch. (From Ter Horst *et al.*, 1981.)

The most systematic single rotational data are available for formaldehyde in its $^1A_2$ electronically excited state. Tang *et al.* (1977) obtained quantum yields for the $2^3 4^1$ vibronic band by comparing absorption and fluorescence excitation spectra. Already in

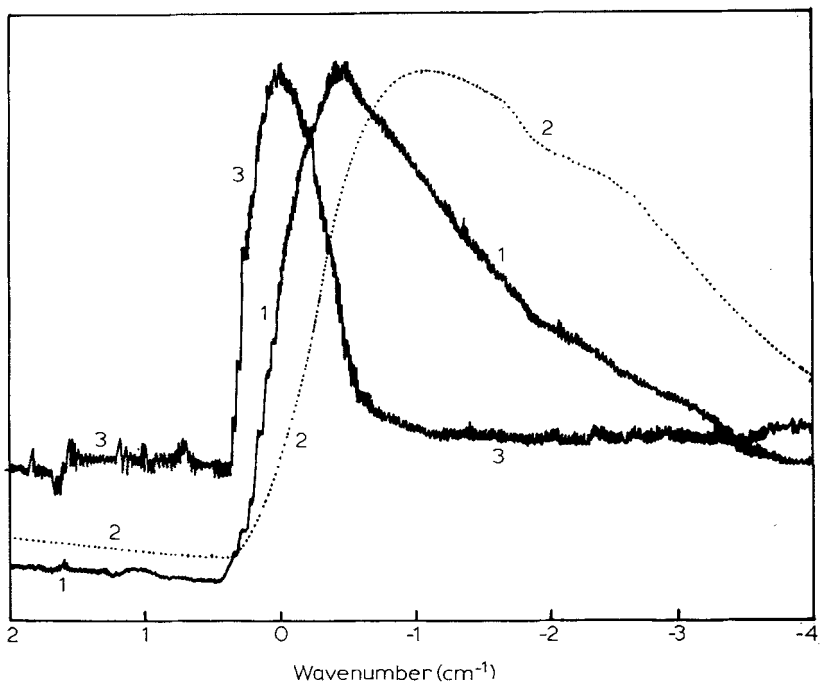

FIG. 2. A set of spectra for the 0–0 band of pyrazine vapour. (1) Fluorescence excitation (at 9.4 mTorr pressure), (2) absorption, (3) quantum yield. (From Baba *et al.*, 1980.)

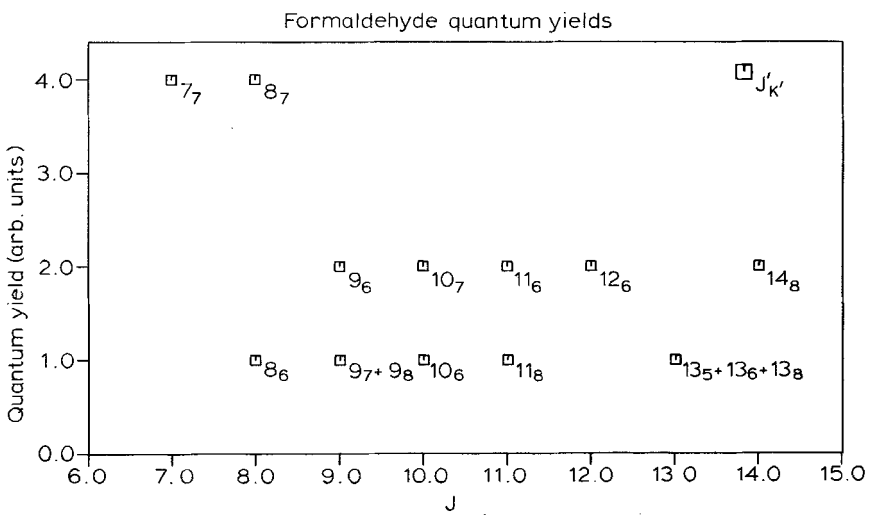

FIG. 3. Single rotational level quantum yields of the $2^3 4^1$ vibrational band of the $^1A_2$ electronic state of formaldehyde. (From Tang *et al.*, 1977.)

this early measurement a fluctuation of yields by a factor of 4 was noted and tentatively attributed to a Coriolis interaction although the interacting level was not identified. The quantum yields are shown in *Figure 3*. The $2^2\,4^1$ band was also investigated by these authors but they reported only little variation (20%) in quantum yields.

Weisshaar and Moore (1979) examined by 4^0 vibronic state in considerable detail. Their data are plotted versus the rotational quantum numbers J and K_{-1} in *Figures 4 and 5* respectively. The lifetimes vary from 66 ns to 4.2 μs and the authors claim that there is no systematic variation with J', K' or E'_{rot}. By inspection of *Figure 5* one can see that there is a general trend towards increasing decay rates with increasing K quantum number. Within each K level the lifetimes do not vary erratically but rather go through maxima or minima. This is shown in *Figure 6* for the $K' = 9$ levels. The decay rates go through a maximum at $J = 13$, decrease to $J = 17$ and again increase to $J = 21$. For most of the other level groups a similar trend can be observed. Another feature can be seen from *Figure 4*. For J groups up to 8 the decay rates increase with K.

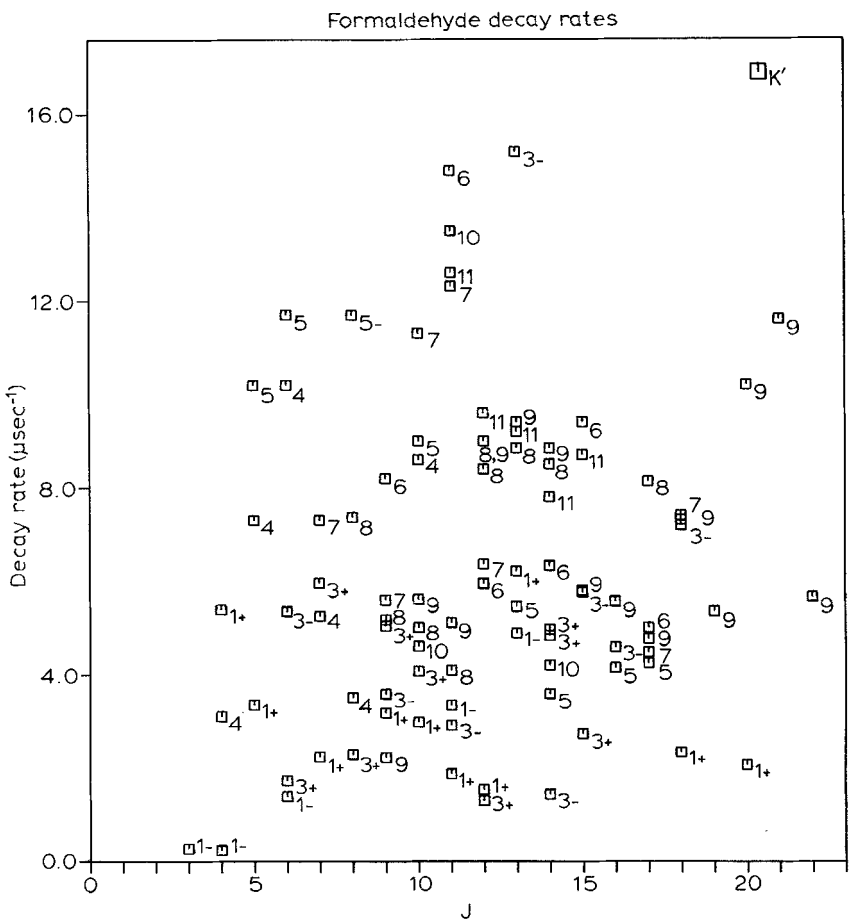

FIG. 4. Single rotational level decay rates of the 4^0 vibrational band of formaldehyde plotted versus J'. The numbers at the points are the K'_{-1} quantum numbers. (Data from Weisshaar and Moore, 1979.)

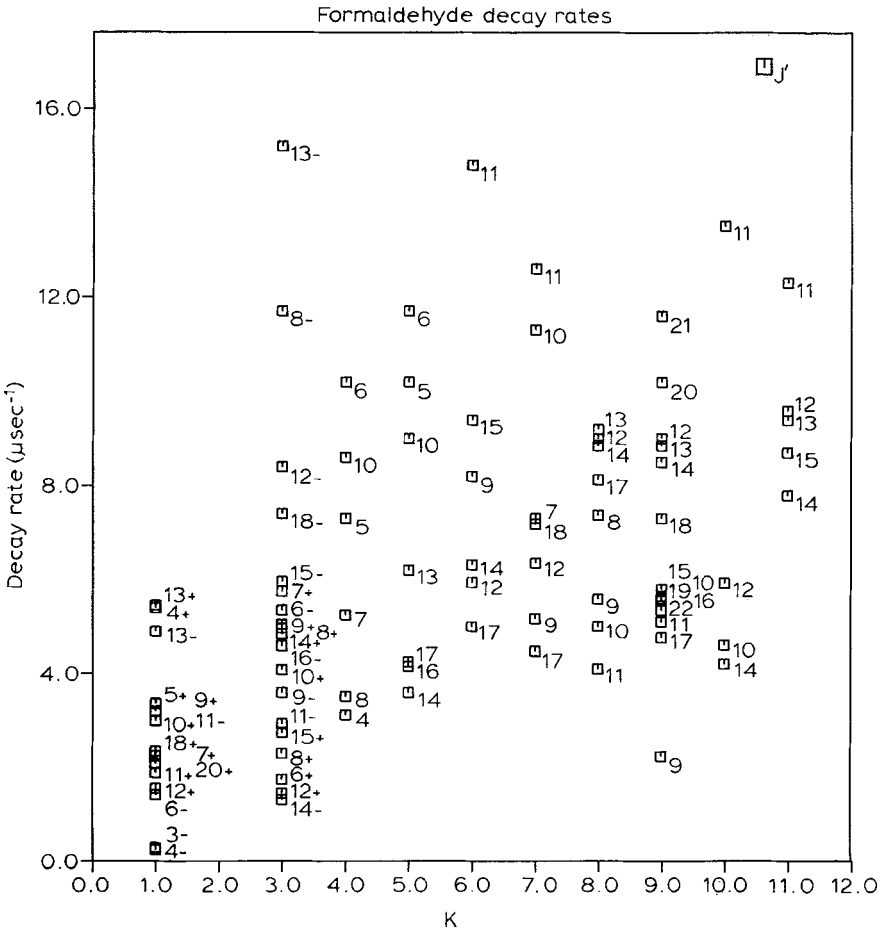

FIG. 5. Single rotational level decay rates of the 4^0 vibrational state of formaldehyde plotted versus K'_{-1}. The numbers at the points are the J' quantum numbers. (Data from Weisshaar and Moore, 1979.)

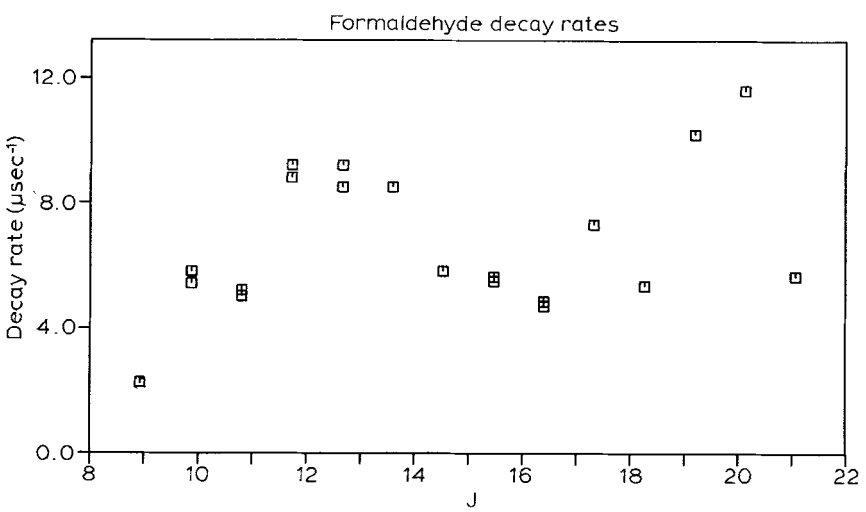

For the $K = 9$ and 10 groups the decay rates go through maxima whereas for higher J groups there is first a maximum and then a minimum with increasing K quantum number.

Later Weisshaar and Moore (1980) reported single rotational lifetimes for the 4^1 vibronic band, which are shown in *Figures 7 and 8*. They see no significant trend in these plots besides a general increase of decay rates with J and K. For the $K = 2$ group the rates increase up to $J = 10$ and then decrease again. All these room temperature measurements were carried out close to the 'zero pressure' regime which is of the order of one milliTorr. Luntz (1978) measured three grouped lifetimes in an effusive beam which agree well with those mentioned above.

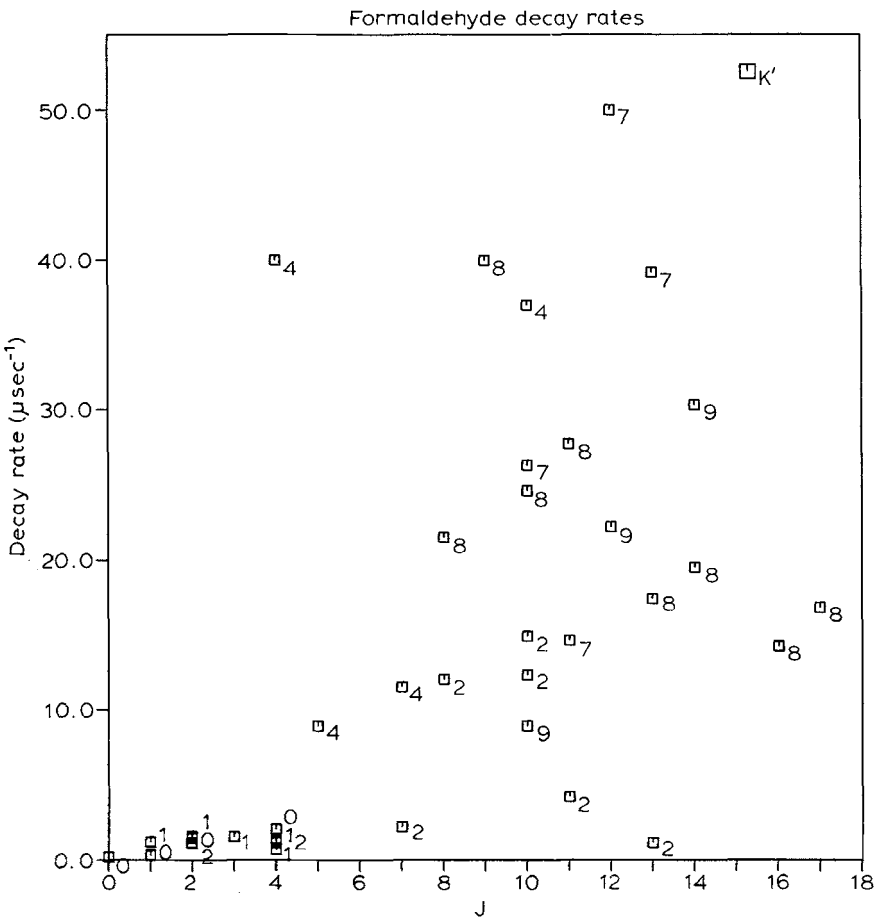

FIG. 7. Single rotational level decay rates of the 4^1 vibrational state of formaldehyde plotted versus J'. The numbers at the points are the K'_{-1} quantum numbers. (Data from Weisshaar and Moore, 1980 and Henke *et al.*, 1982a.)

FIG. 6 (*Left*). Single rotational level decay rates of the 4^0 vibrational state of formaldehyde with $K'_{-1} = 9$ plotted versus J'. (Data from Weisshaar and Moore, 1979.)

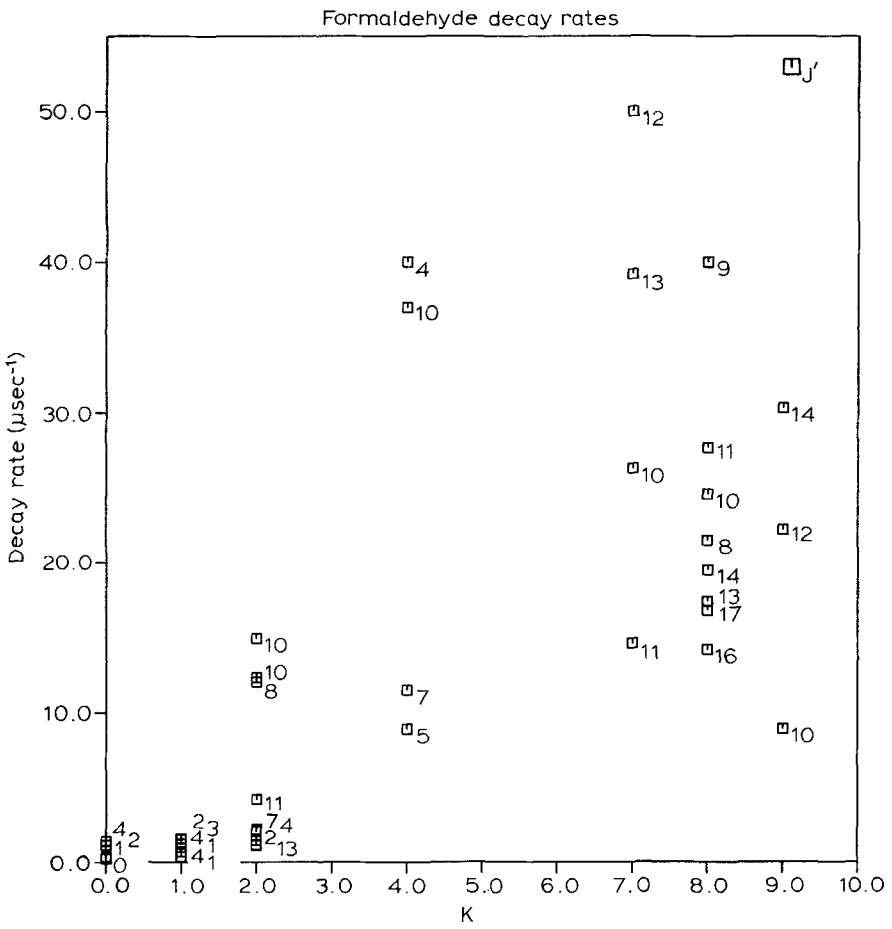

FIG. 8. Single rotational level decay rates of the 4^1 vibrational state of formaldehyde plotted versus K'_{-1}. The numbers at the points refer to the J' quantum numbers. (Data from Weisshaar and Moore, 1980 and Henke *et al.*, 1982a.)

It is pointed out that there could be a correlation between the single rotational decay rates and magnetic optical activity in the 4^1 vibrational state of formaldehyde. Most of the rovibronic states which have decay rates of more than 10 μs^{-1} were reported to be active in a magnetic rotation spectrum (Ramsay and Till, 1979) whereas those with decay rates below 10 μs^{-1} are not active. However, this correlation may be misleading since most of the fast decay rates correspond to levels which have more than 400 cm^{-1} of rotational energy, whereas the slow decays are observed for levels with less than 300 cm^{-1} of rotational energy.

Shibuya *et al.* (1981) obtained single rotational level quantum yields for the 4^1 vibronic state and they are shown in *Figures 9 and 10.* The yields vary by more than a factor of 40. They decrease rapidly with increasing J' or K' and level off at about $J' = 8$ and $K' = 6$. Using these quantum yields and the lifetimes from Weisshaar and Moore (1980) it is possible to calculate the radiative decay rates which are shown in *Figures 11 and 12.*

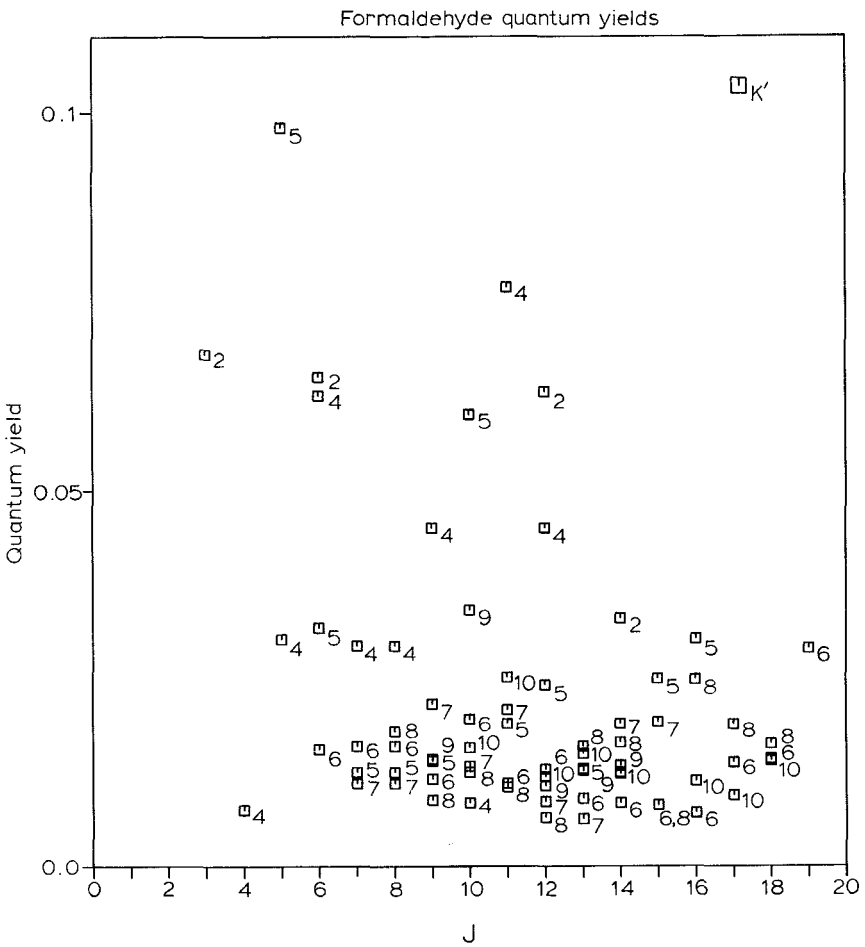

FIG. 9. Single rotational level quantum yields of the 4^1 vibrational state of formaldehyde plotted versus J'. The numbers at the points refer to the K'_1 quantum number. Not given in the figure are the values for the 2_2 and 4_2 levels of 0.322 and 0.2 respectively because they are far out of the range. (Data from Shibuya *et al.*, 1981.)

Selzle and Schlag (1979) reported the first lifetime measurement in a hypersonic jet on the $2^2\,4^1$ band with 2470.6 cm^{-1} excess energy. One advantage of the jet is the very low collision rate after the isentropic expansion. Furthermore the low rotational 'temperatures' in a jet result in a much less congested spectrum so that clean single rotational excitation is easily achieved. Particularly low rotational quantum numbers can be excited and these are difficult to see precisely with room temperature measurements. Here room temperature and jet work nicely complement each other. In *Figure 13* the experimental data for the $2^2\,4^1$ band are shown in the upper part of the figure. The rates do not fluctuate much (20%), but generally the decay rates increase with K within each J group.

The lifetimes of single rotational levels in the 4^1 and 4^3 bands of formaldehyde with 124.6 and 947.9 cm^{-1} excess energy respectively were measured by Henke *et al.*

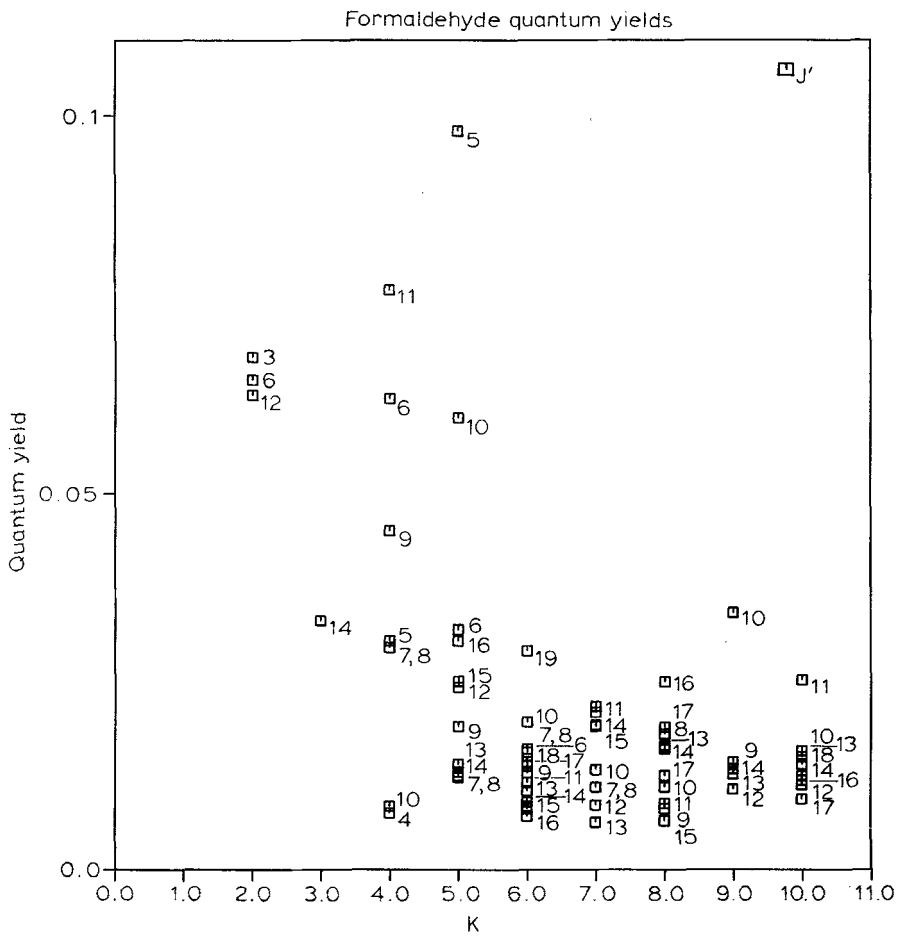

FIG. 10. Single rotational level quantum yields of the 4^1 vibrational state of formaldehyde plotted versus K'_{-1}. The numbers at the points refer to the J' quantum number, without the 2_2 and 4_2 values of 0.322 and 0.2 respectively. (Data from Shibuya *et al.*, 1981.)

(1982a). Since the lifetimes are much longer than for the $2^2\,4^1$ band found by Selzle and Schlag (1979) a careful consideration of collisions in a hypersonic jet is necessary. If one assumes as a worst case that the translational 'temperature' is equal to the rotational 'temperature' of 17 K which could be accurately determined by comparison with theoretical spectra, one obtains a time between collisions of 5 μs. The actual collision rate will be even lower since translational cooling is more efficient than rotational cooling. In this rough calculation the low energy collision cross-sections are assumed to be as large as their room-temperature values. The validity of this assumption was checked experimentally by comparison with room temperature lifetimes since a few lines were measured in the jet and at room temperature. These are compared in *Table 2*. It can be seen that the lifetimes agree well in the cases where clean excitation was achieved at room temperature. But when several rotational states were

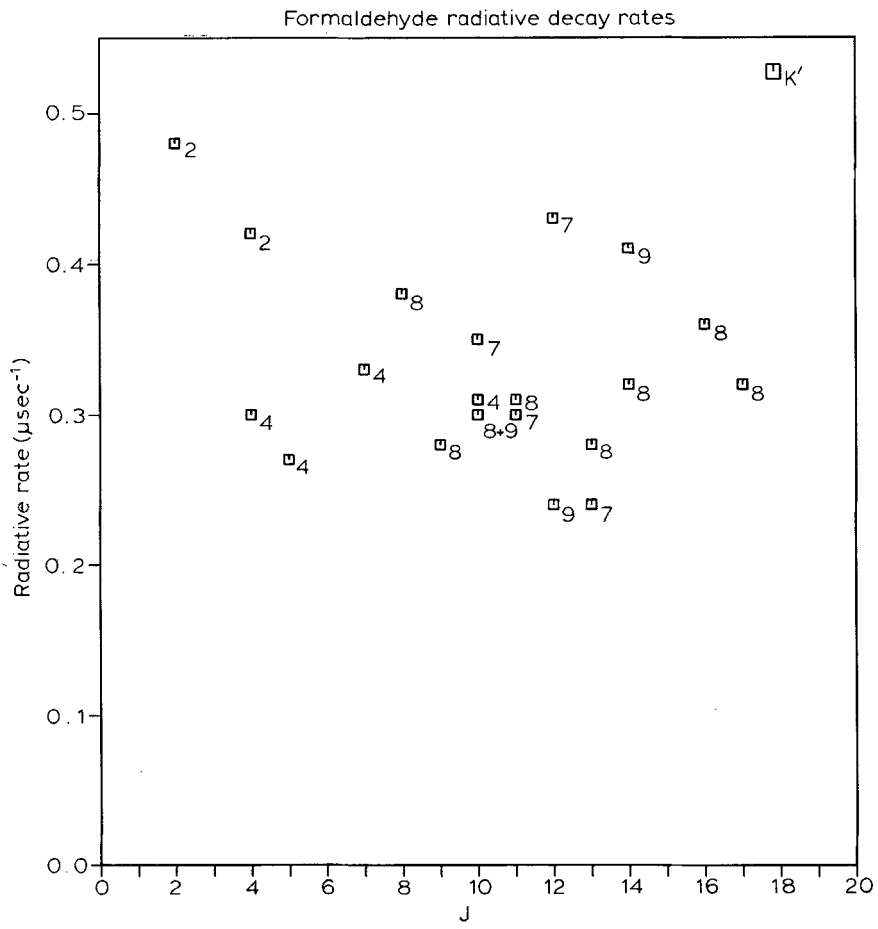

FIG. 11. Single rotational level radiative decay rates for the 4^1 vibrational state of formaldehyde plotted versus J'. The numbers at the points refer to the K'_{-1} quantum number. (Data from Shibuya *et al.*, 1981 and Weisshaar and Moore, 1980.)

excited (e.g. the 0_{00} and 3_{03}) the lifetimes differ. In the jet experiments it is possible to determine the 0_{00} and 3_{03} rotational level lifetimes individually.

The 4^1 decay rates are shown in *Figure 14*. Note that the jet decay rates are also displayed in those figures together with the room-temperature decay rates. In order to extract the non-radiative decay rate from the experimentally determined decay rates the radiative decay rate must be subtracted.

$$K_{NR} = \frac{1}{\tau_{NR}} = \frac{1}{\tau_{exp}} - \frac{1}{\tau_R} \tag{1}$$

In *Figure 14* the decay rates are plotted versus rotational energy. It is possible to detect a general trend from this plot. The 0_{00} decay rate is the slowest. Going to higher energy in general increases the decay rates. Besides this trend there is a fluctuation of rates. Some experimental error bars are plotted in *Figure 14* from which one can conclude

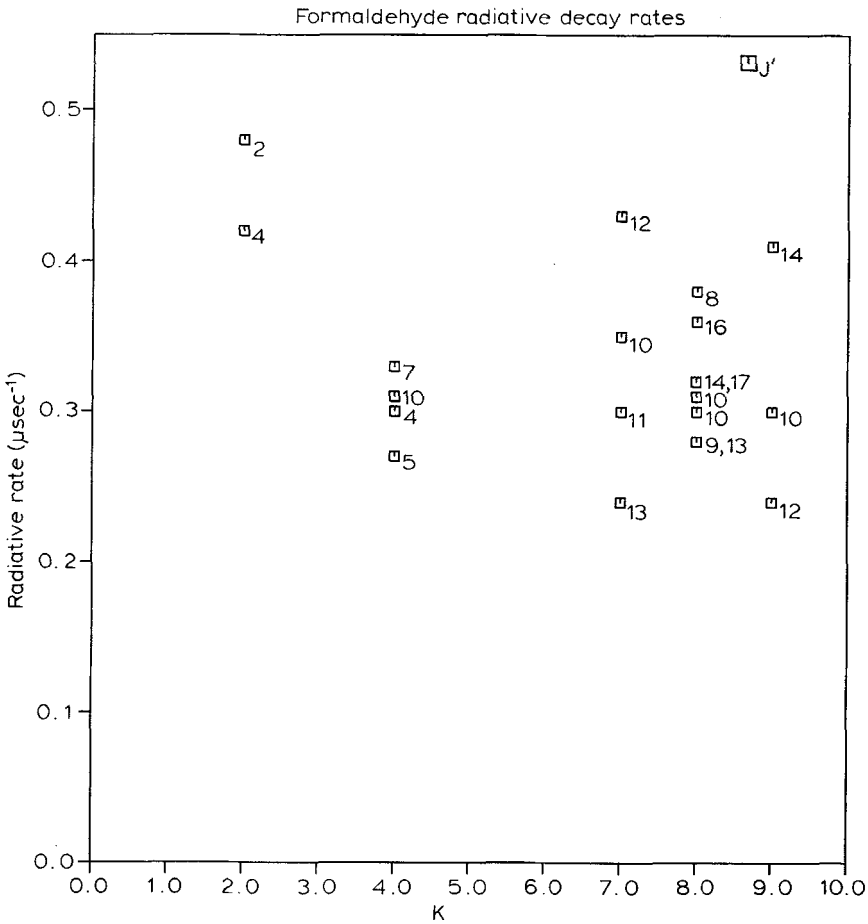

FIG. 12. Single rotational level radiative decay rates for the 4^1 vibrational state of formaldehyde plotted versus K'_{-1}. The numbers at the points refer to the J' quantum number. (Data from Shibuya *et al.*, 1981 and Weisshaar and Moore, 1980.)

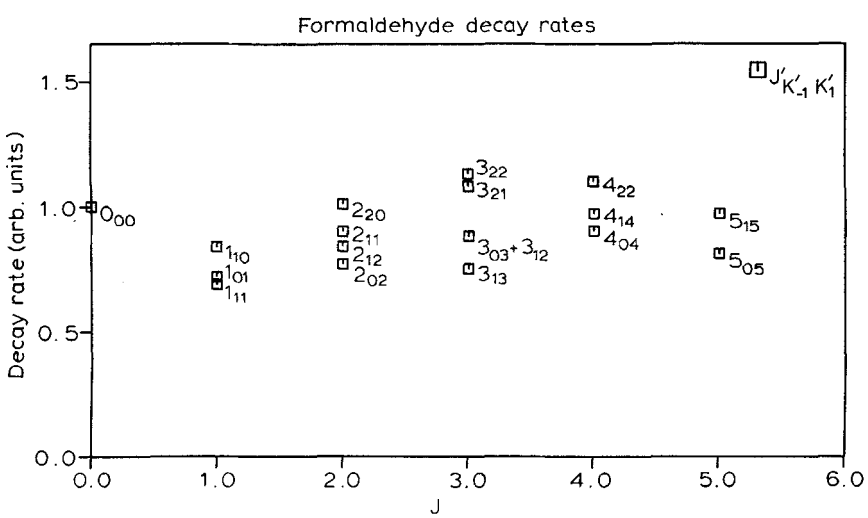

TABLE 2. Comparison of lifetimes measured at room temperature and in the jet for the 4^1 band of formaldehyde*

$J'_{K'_{-1}K'_1}$	τ *Room temperature* (μs)	τ *Jet* (μs)
0_{00}	3.10	4.67
3_{03}		0.1
1_{01} (← 2_{12})	2.85	2.80
1_{01} (← 1_{10})	2.66	2.34
4_{04}	0.563	0.70
5_{23}		
2_{02}	0.86	0.875
$13_{2,13}$		

* Data from Weisshaar and Moore (1980) and Henke *et al.* (1982a).

that these fluctuations are not merely an artefact due to the error of lifetime determinations. Especially noteworthy are the 1_{10} and 1_{11} rotational levels, whose lifetimes differ by a factor greater than 3 but whose difference in rotational energy is only 0.12 cm^{-1}.

In *Figures 15 and 16* the decay rates are plotted versus the rotational quantum number J' and K'_{-1}. The decay rates were normalized by dividing them by the decay rate of the 0_{00} level. In the plot versus J an increase of rates up to $J = 3$ can be found. In general the decay rates do not depend on K for each different J. In the plot versus K the

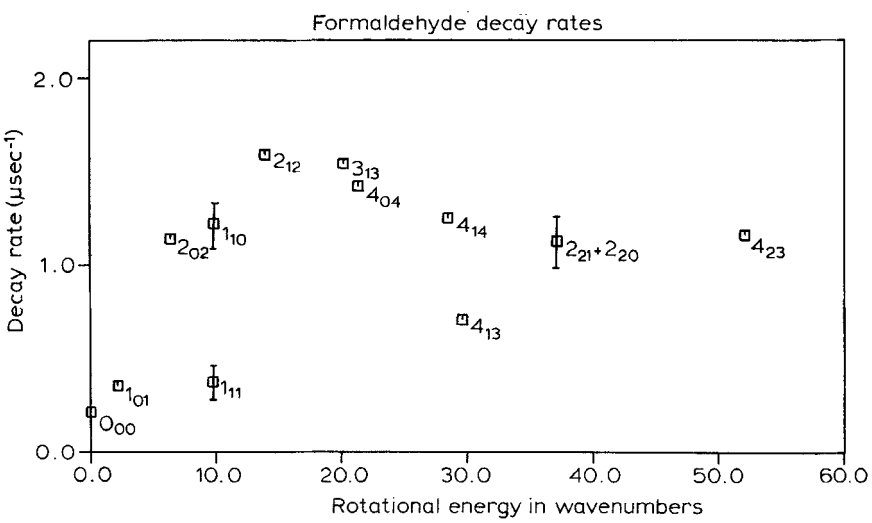

FIG. 14. Single rotational level decay rates of the 4^1 vibrational state of formaldehyde measured in a hypersonic jet. (From Henke *et al.*, 1981.)

FIG. 13 (*Left*). Single rotational level decay rates of the 2^2 4^1 vibrational state of formaldehyde measured in a hypersonic jet. (Data from Selzle and Schlag, 1979.)

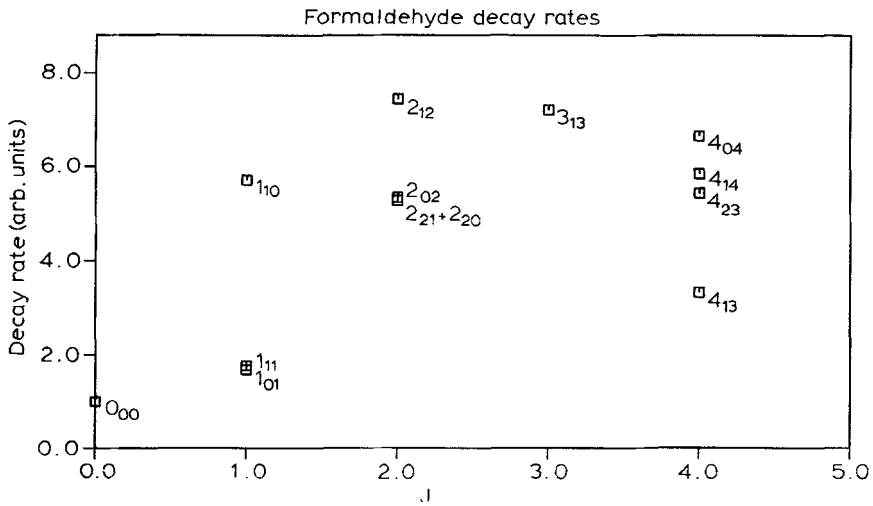

FIG. 15. Single rotational level decay rates of the 4^1 vibrational state of formaldehyde measured in a hypersonic jet. (From Henke *et al.*, 1982a.)

decay rates again increase with K but no systematic variation with J for a single K can be found.

The 4^1 spectra in *Figure 17* are compared to a calculated spectrum. This spectrum was obtained with an asymmetric rotor program, the constants were taken from Job *et al.* (1969). The *ortho-para* nuclear hyperfine states were shown not to relax but stay at their room temperature ratio. We estimate the rotational temperature to be 17 K and 2 K for the He and Ar carrier gas, respectively. Under our conditions, Ar cools the molecules to lower rotational temperatures than He, an Ar pressure below 0.1 atm is

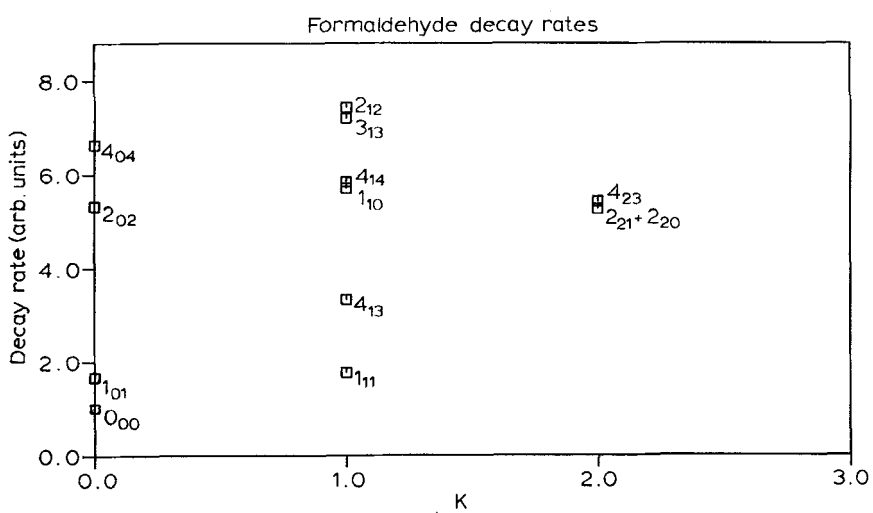

FIG. 16. Single rotational level decay rates of the 4^1 vibrational state of formaldehyde measured in a hypersonic jet. (From Henke *et al.*, 1982a.)

sufficient for a rotational temperature of 17 K. The vibrational temperature was estimated to be 150 K by comparing the intensities of the 4_0^1 band with the 4_1^0 hot band and assuming the same Franck–Condon factors.

In the experimental spectrum of *Figure 17b* two transitions are missing. Both these transitions originate from the same upper state: 3_{03}. Three transitions are allowed from the 3_{03} upper state: the ${}^pP_1$ (4) transition to 4_{14}, the ${}^pR_1$ (2) to 2_{12} and ${}^pQ_1$ (3) to 3_{12}. The first two are not observed in the spectrum. The third transition overlaps with the ${}^pP_1$ (1) transition, and it cannot be decided if it is present or not. One can take the missing

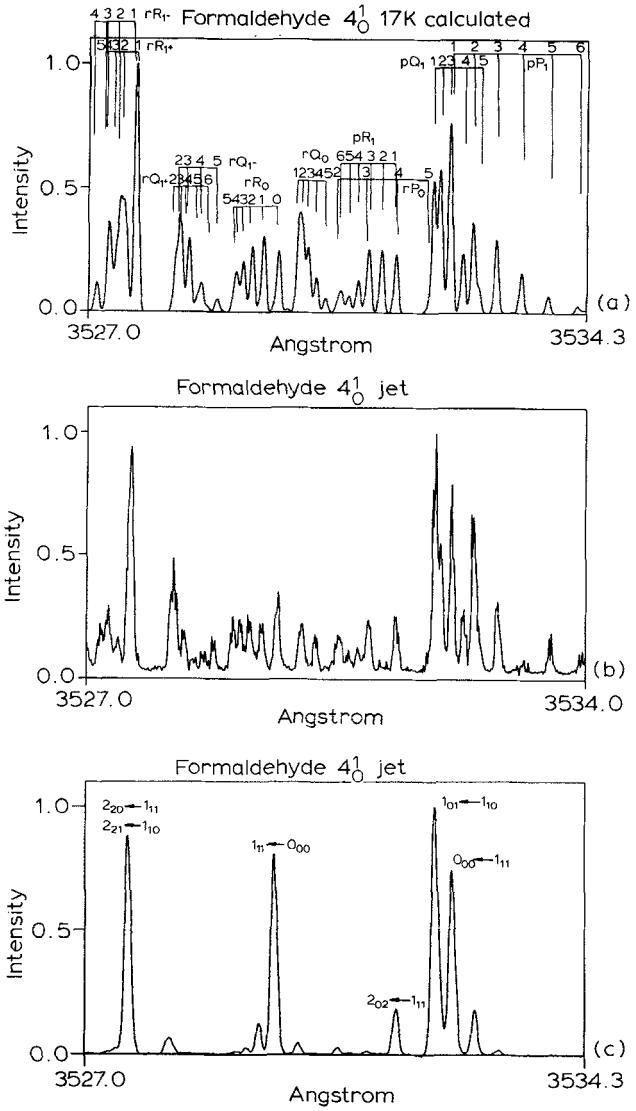

FIG. 17. Fluorescence excitation spectrum of the 4^1 band for formaldehyde in a hypersonic jet. (a) Calculated spectrum, (b) formaldehyde seeded in 0.5 atm of helium, (c) formaldehyde seeded in 0.5 atm of argon. (From Henke *et al.*, 1982a.)

transitions as evidence for a low quantum yield which is caused by strong coupling to a non-radiating state. Since

$$\tau_{exp} = \Phi\tau_R \tag{2}$$

where τ_R is the radiative lifetime, one expects a short lifetime for this state. Note that for the determination of Φ one assumes here that the absorbed intensity is as large as calculated theoretically. This is a valid assumption which has been checked experimentally by Fairchild *et al.* (1980). The transitions ${}^rQ_0$ (5), ${}^rQ_0$ (3), ${}^rQ_{1-}$ (4) and ${}^rR_{1-}$ (2) are all missing, too, so the states 5_{14}, 3_{12}, 4_{22} and 3_{21}, respectively, probably have low quantum yields and short lifetimes. Another possible explanation for the missing transitions could be a perturbation in absorption.

The 4^3 decay rates are shown in *Figures 18 and 19*. It can be seen that within each J group the rates decrease with increasing K. It has been shown by Henke *et al.* (1981b) that this is expected if a Coriolis interaction takes place (*see* the section on theory). In fact an interacting level, the v_6 vibrational state was found whose origin is only 52 cm^{-1} below the 4^3 origin as can be seen from *Figure 20*. Note that the intensities in the 6_0^1 band decrease towards the high energy side and the reverse is true for the 4_0^3 band. The discrepancy between the calculated and measured spectrum in *Figure 20* is large. The line positions match well, but the intensities do not. If one attributes this to the drastically different quantum yields of individual rotational states and assumes that the quantum yield is proportional to the experimentally determined lifetimes, and corrects the intensities to a constant quantum yield, then the agreement between calculated and measured spectra is better. The calculated spectra were obtained from an asymmetric rotor program with rotational constants taken from Job *et al.* (1969) for the 4_0^3 band and from Henke *et al.* (1982a) for the 6_0^1 band.

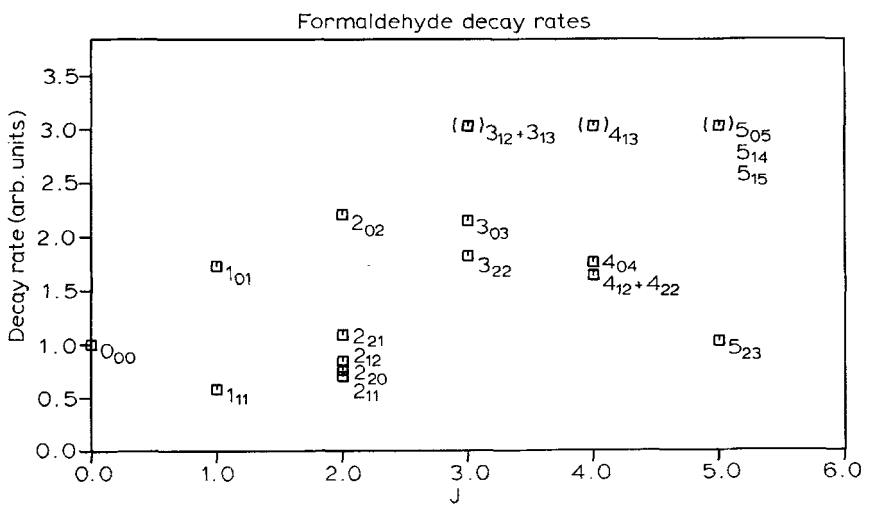

FIG. 18. Single rotational level decay rates of the 4^3 vibrational state of formaldehyde in a hypersonic jet. The values in brackets are estimated decay rates only, as mentioned in the text. (From Henke *et al.*, 1982a.)

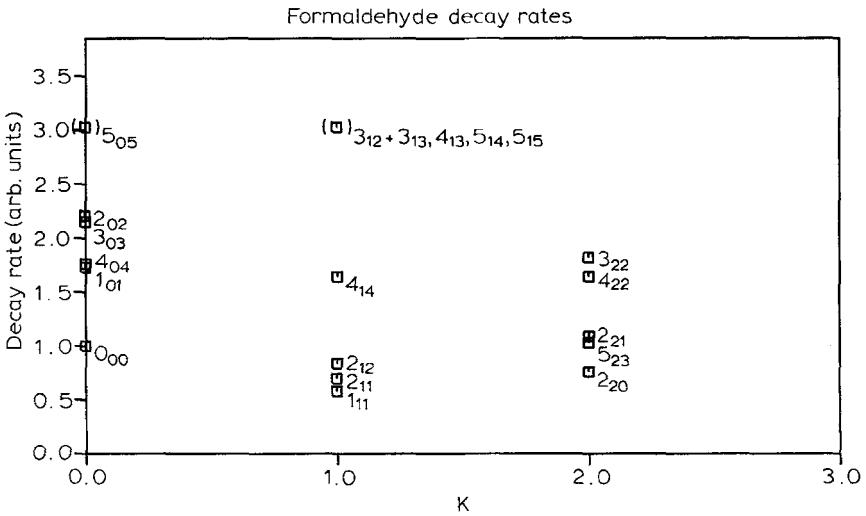

FIG. 19. Same as *Figure 18* but plotted against K'_{-1} instead of J'.

Deuterated formaldehyde

Weisshaar and Moore (1980) and Shibuya *et al.* (1981) reported lifetime and quantum yield measurements for the 4^0, 4^1, 4^3 and $2^1\,4^3$ band of deuterated formaldehyde. Those rotational levels for which single rotational excitation was achieved are shown in *Table 3*, and the data for the $2^1\,4^3$ band are displayed in *Figures 21 and 22*. In general the lifetimes are longer than in protonated formaldehyde and closer to the radiative lifetime. Secondly the lifetimes fluctuate much less. But if the vibrational excess energy is increased the fluctuation in lifetimes increases. The lifetimes vary by a factor of 4 in the $2^1\,4^3$ band with 1847 cm^{-1} of vibrational excess energy. This is in contrast to protonated formaldehyde for which much less fluctuation was found at high excess energy; the lifetimes of the $2^2\,4^1$ band change by only 20%. For some rotational levels

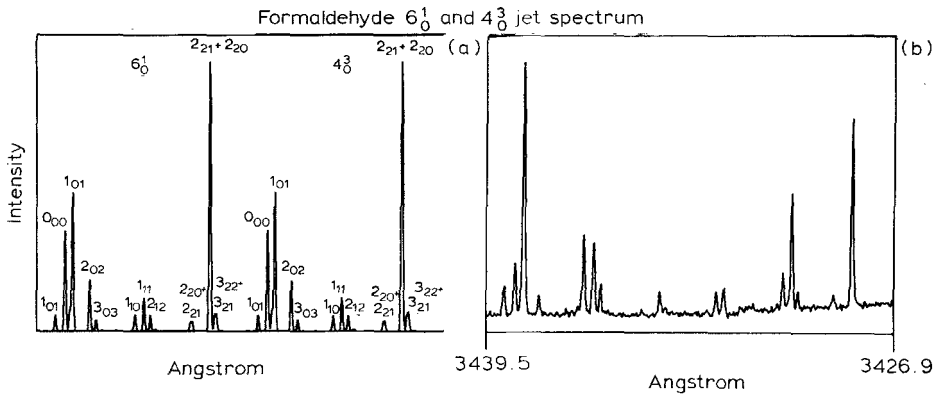

FIG. 20. Fluorescence excitation spectrum of the 4^3 and 6^1 vibrational bands of formaldehyde in a hypersonic jet. (a) Calculated spectrum, (b) experimental. (From Henke *et al.*, 1982a.)

of the 4^1 band, lifetimes and quantum yields were measured so that radiative lifetimes can be obtained, which are also shown in *Table 3*.

S_1 aromatics

Recently Coveleskie *et al.* (1981) studied vibrational redistribution in 10 different S_1 aromatics in the collision-free regime. Redistribution first becomes important with between 1000–2000 cm^{-1} of excess energy. From S_1 rotational level widths in high resolution absorption studies, redistribution lifetimes were identified and the importance of rotational levels to redistribution in these systems was shown.

Quantum beats

One of the elementary steps in a photochemical reaction sequence is the coupling of the initial excited states to final accepting states, a process about which little is known in spite of a decade of intense effort. Most tests are gross comparisons of measured or deduced lifetimes averaged over many states. State-by-state tests of individual states for

TABLE 3. Lifetimes of single rovibronic levels of D_2CO*

J'	K'	τ (μs)	Φ (arb. units)	τ_R (arb. units)
4^0	*band*	$E_{vib} = 0$ cm^{-1}		
14	2	7.6		
5	2	6.6		
19	8	8.1		
14	10	6.2		
16	8	7.2		
13	8	5.54		
4^1	*band*	$E_{vib} = 69$ cm^{-1}		
12	9	5.08	1.18	4.31
13	9	4.96	1.58	3.14
14	9	4.14	1.05	3.94
15	9	4.92	2.23	2.21
16	9	5.06	0.98	5.16
15	5	4.5	1.35	3.33
10	4	6.9		
14	4	6.3		
5	5	6.5		
13	5	6.5		
16	5	5.0		
4^3	*band*	$E_{vib} = 669$ cm^{-1}		
5	5	2.46		
11	9	1.97		
12	9	1.31		
13	9	1.09		
14	9	1.62		
14	11	1.79		

* Data from Weisshaar and Moore (1980).

such lateral transitions are largely absent. Ideally one would like to measure under Doppler-free and collision-free conditions the spacing between individually prepared initial and coupled final states, the decay rates, the coupling matrix elements, etc. One approach to this is to look for quantum beats.

The search for quantum beats in polyatomic molecules is old. Recently Chaiken *et al.* (1979) and Gurnick *et al.* (1981a) have observed quantum beats in the fluorescence of biacetyl and methylglyoxal in its first excited singlet state. They show that they are true intramolecular quantum beats due to coupling between singlet and triplet in contrast to

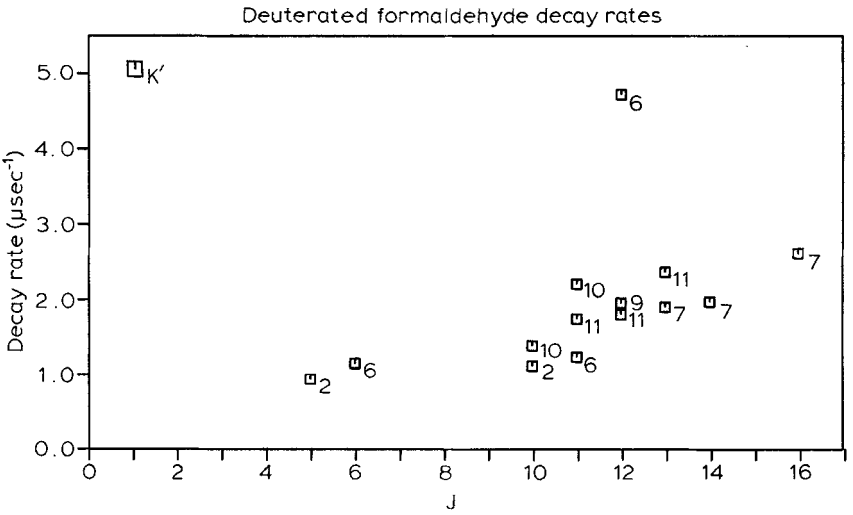

FIG. 21. Single rotational level decay rates of the $2^1 4^3$ vibrational band of deuterated formaldehyde. (Data from Weisshaar and Moore, 1980.)

quantum beats in atoms and diatomics. Furthermore the states involved are very narrow compared to the coupling matrix elements and a coherent superposition of states is created by the laser pulse. They analysed quantum beats from many rotational states and found that the singlet–triplet coupling energies lie between 0 and 12 MHz (*Figure 23*). The singlet–triplet spacing was found to vary between 0 to 44 MHz. They also determined lifetimes of individual rotational states and these are given in *Table 4*. In *Figure 24* the dependence of quantum beats on the distance from the nozzle is shown.

Very recently quantum beats have been found in triatomics. Brucat and Zare (1981) observed Zeeman beats in the NO_2 $^2B_2$ excited state. They studied the population and alignment decay of individual hyperfine levels. Sharfin *et al.* (1981) observed quantum beats in fluorescence of individual rovibronic states of the SO_2 $\tilde{C}(^1B_2)$ state in a hypersonic beam.

Another method for the study of singlet–triplet coupling was reported by Lombardi *et al.* (1980). Level anticrossing and optical radio frequency double resonance techniques were used to study singlet–triplet interactions of single rotational states of S_1 glyoxal. Due to space limitations this will not be discussed here.

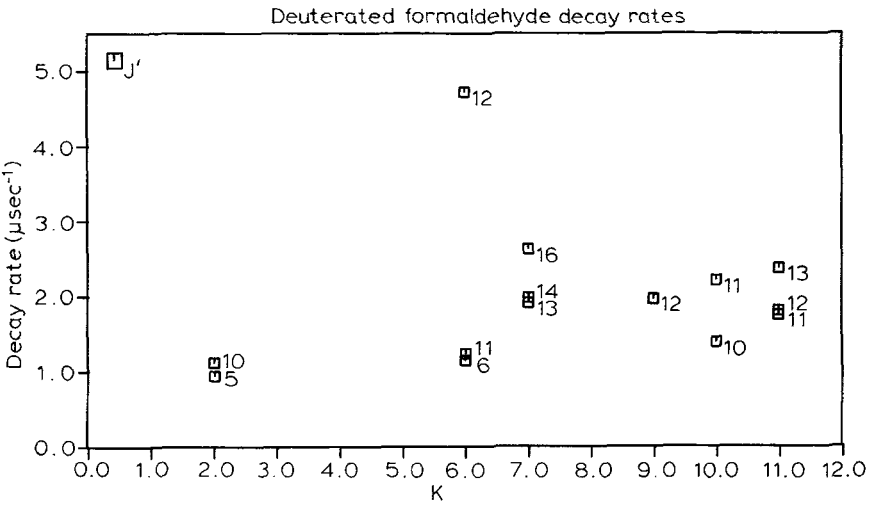

FIG. 22. Same as *Figure 21* but plotted against K'_{-1} instead of J'.

The effect of collision and magnetic field on the quantum beat in biacetyl was investigated by Henke *et al.* (1981a). By comparing the beat and its Fourier transform to the theoretical model (*see* theory section) they obtained the lifetime, the spacing between the coupled states, the coupling energy and the dephasing rate constant. In *Figure 25* the quantum beat and its Fourier transform for the 2_{02} excited state in the vibrational band 273 cm^{-1} above the origin of the first singlet of biacetyl are shown. The assignment of the 2_{02} rotational state is not absolutely certain. The 273 cm^{-1} vibrational band was simulated with an asymmetric rotor program and rotational

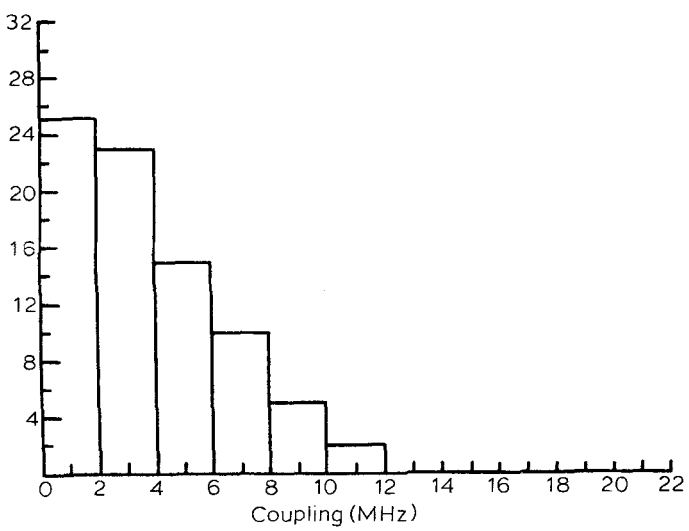

FIG. 23. A histogram of singlet–triplet coupling energies for methylglyoxal 22 000 cm^{-1} above its S_0 ground state. (From Gurnick *et al.*, 1981.)

constants which were obtained from comparing the 0 cm^{-1} and 160 cm^{-1} vibrational bands. These constants agree well with those calculated from the moments of inertia of a postulated molecular structure. The experimental spectrum of the 273 cm^{-1} band is perturbed and cannot be compared well to the calculated spectrum. However, there is some agreement and from this the 2_{02} rotational assignment for the excited state results.

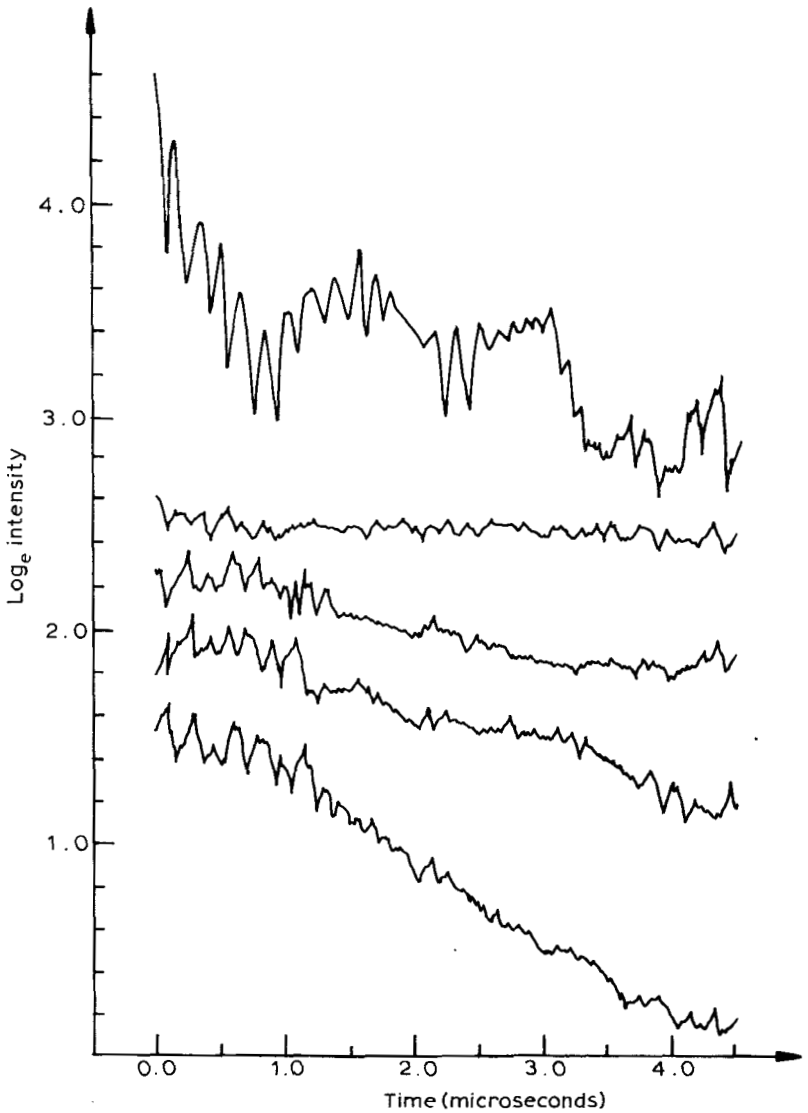

FIG. 24. Quantum beat patterns of the 2_{11} rotational state in the 160 cm^{-1} excess energy vibrational level of biacetyl. The distances from the nozzle are 186, 140, 93, 70 and 47 nozzle diameters from top to bottom. All decays at distances closer than 186 nozzle diameters are divided by the one which was obtained at 186 nozzle diameters. (From Chaiken *et al.*, 1981.)

The energy relaxation time which is probably shortened by collisions was determined from the fluorescence decay. The value for this particular beat is 1.25 μs, the rate 0.80 MHz. If the linewidth is only due to energy relaxation, it should be

$$\Delta\nu = \frac{1}{2\pi\tau} = 0.13 \text{ MHz}.$$

In the Fourier spectrum of the time decay a linewidth of 0.72 MHz (FWHM) was obtained.

The linewidth is more than five times broader than expected from a pure energy relaxation, indicating that there is a large amount of phase relaxation. This phase relaxation is probably due to the fact that the jet is not collision free at the position of the measurement, 100 nozzle diameters from the nozzle. The linewidth of collisional dephasing ν_c depends on the collision frequency Z.

$$\Delta\nu_o = \frac{Z}{\pi} \tag{3}$$

The collision rate per molecule per unit of distance is a function of temperature, density, mean velocity and collision cross-section. If one applies the equations for an adiabatic expansion one obtains

$$\Delta\nu_c = (\Delta\nu_c)_0 \left(\frac{X}{D}\right)^{-8/3} \tag{4}$$

TABLE 4. Lifetimes of single rovibronic levels in methylglyoxal and biacetyl*

$J'_{K'_1 K'_1}$	τ (μs)
Methylglyoxal	$E_{vib} = 85$ cm^{-1}
1_{01}	1.5
1_{11}	2.1
1_{10}	1.9
2_{02}	3.0
2_{11}	1.9
Methylglyoxal	$E_{vib} = 137$ cm^{-1}
1_{01}	1.9
1_{10}	1.9
2_{11}	2.8
2_{21}	1.7
Biacetyl	$E_{vib} = 0$ cm^{-1}
0_{00}	5.0
1_{10}	3.7
2_{11}	8.7
Biacetyl	$E_{vib} = 160$ cm^{-1}
1_{11}	5.0
2_{02}	4.4
2_{11}	4.1

* Data from Chaiken *et al.* (1981).

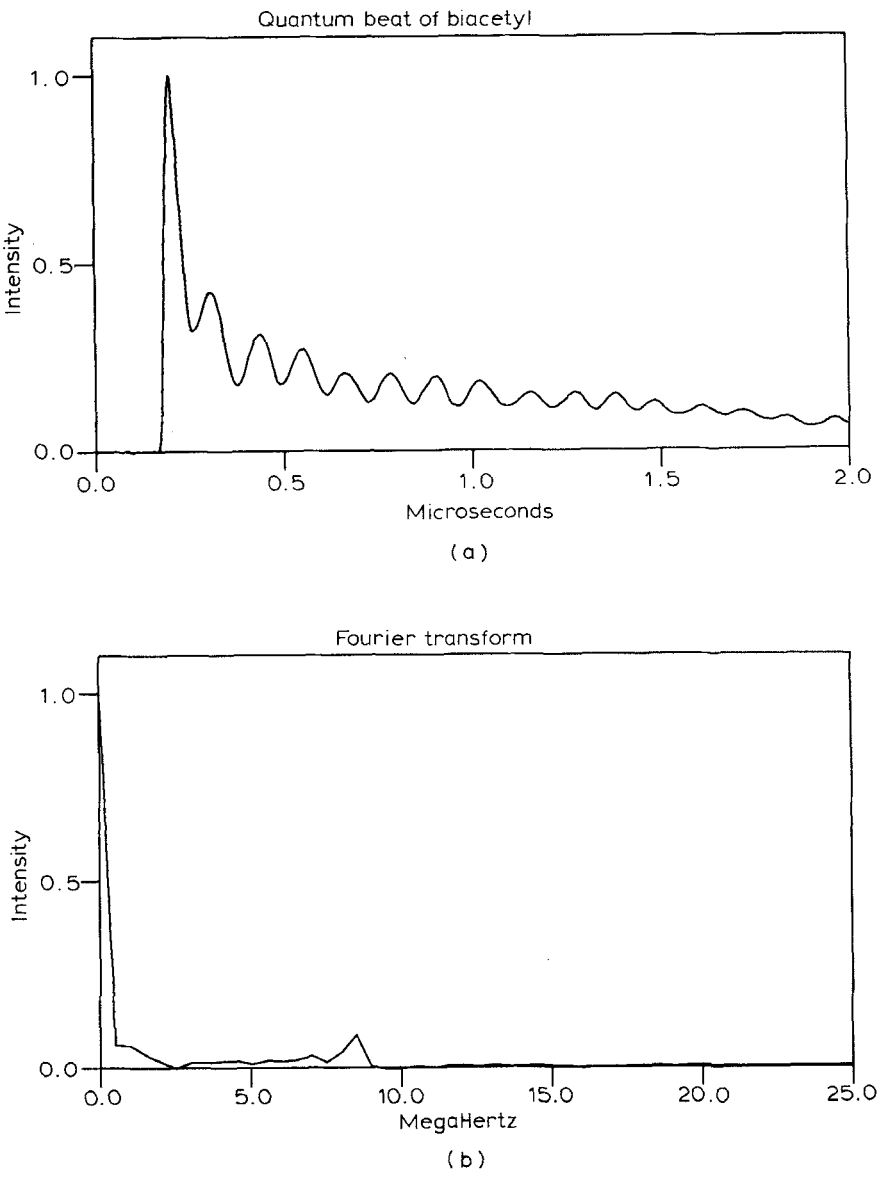

FIG. 25. (a) Quantum beat of the 2_{02} rotational state in the 273 cm^{-1} excess energy vibrational level of biacetyl seeded in 5 atm of helium at 100 nozzle diameters from a pulsed 200 μm diameter nozzle. (b) Fourier transform of (a) without modification.

This equation only holds until the free jet is formed, where the collision rate starts to be too low to establish equilibrium. This point is reached at about 30 nozzle diameters under our experimental conditions (pressure 3.5 atm, nozzle 200 μm). From this point

onwards the temperature and the velocity do not decrease any more, but the density does. So one would expect

$$\Delta\nu_c = (\Delta\nu_c)_0 \left(\frac{X}{D}\right)^{-2} \tag{5}$$

Note that this equation implies that there are collisions to cause dephasing, although there are not enough collisions to establish equilibrium. In *Figure 26* the experimental quantum beats at different nozzle distances are shown and in *Figure 27* the dephasing rate is plotted against the nozzle distance. The two points for the smallest nozzle distance have a large error since the short lifetimes preclude an exact observation of the beat. The curve does not vary in the region between 60 to 150 nozzle diameters in disagreement with expectations. It appears as if the collision frequency does not change beyond a distance of 60 nozzle diameters. It is likely that hot background gas of 4 mTorr pressure produces these collisions. Note that there are several uncertainties in

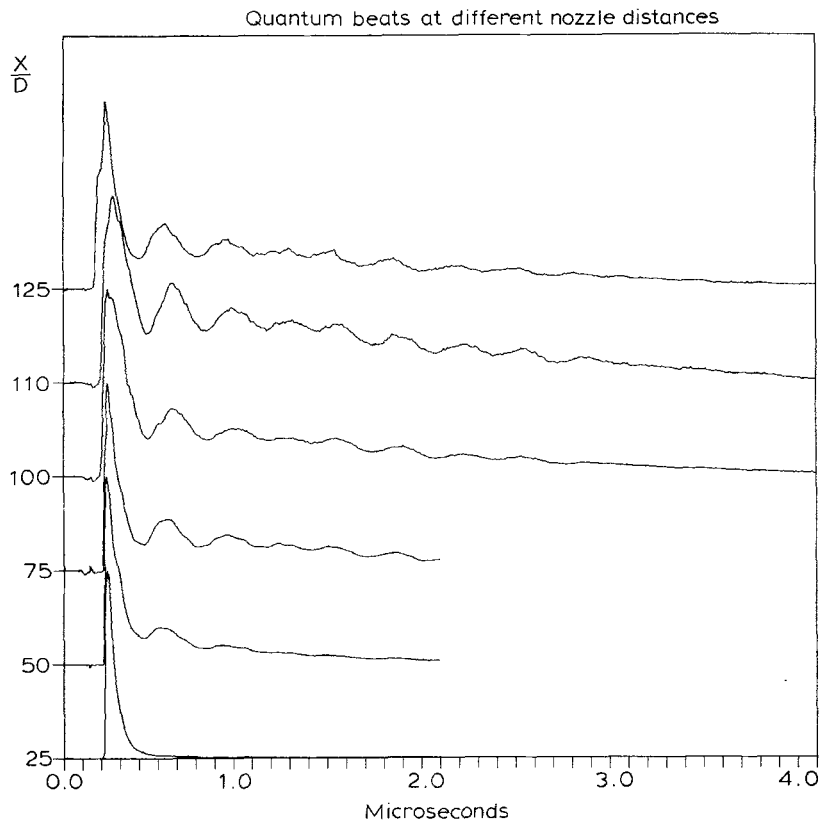

FIG. 26. Quantum beats of the 1_{01} rotational state of the 273 cm^{-1} excess energy vibrational band of biacetyl seeded in 5 atm of helium at different distances from the 200 μm diameter nozzle.

the above calculations, as for example the temperature or energy dependence of the collision cross-section, the non-Maxwellian velocity distribution etc., but this will not influence our conclusions drastically.

A magnetic field was also applied in the study of the quantum beats in biacetyl by Henke *et al.* (1981). If triplets are involved one might expect that the triplet levels shift in energy and therefore the beat frequency, which corresponds to the energy difference between the coupled states, was expected to change. In *Figure 28* we display the quantum beats of the 2_{02} rotational state at different magnetic fields. The highest magnetic field in this figure is 70 Gauss. For a free electron, this field should shift the beat frequency by 210 MHz. But as can be seen from *Figure 28* the beat frequency changes much less. This occurs because the spin is not completely decoupled from the molecular frame. Another possibility is that the M_0 triplet substate is involved which is not influenced by the magnetic field.

Looking again at *Figure 28* one sees that the beat disappears as the magnetic field increases because the fluorescence intensity disappears. The first fast peak, however, is not influenced. This magnetic effect on the fluorescence of biacetyl is very drastic (Henke *et al.*, 1980). A weak field of 70 Gauss is enough to quench most of the fluorescence. Another interesting fact is that the beat becomes less pronounced at 11.2 Gauss, but more pronounced again at 14 Gauss.

THEORY

As discussed in the previous section, recent experiments on SRVL lifetimes of polyatomic molecules indicate that non-radiative (NR) transitions not only differ for various SVL's but are also strongly dependent on the rotational states involved. Thus our present understanding of the radiationless transitions depends upon a correct characterization of all states of the molecule including rotational levels. In this section, the theory of SRVL radiationless transitions will be discussed. Howard and Schlag (1976, 1978a, 1978b, 1980) suggested a systematic approach to the effects of

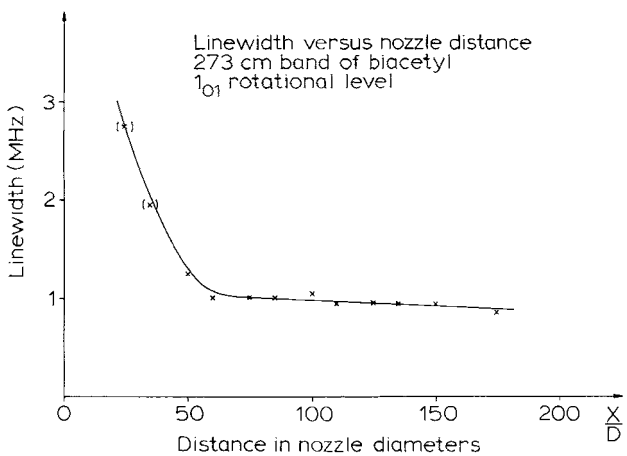

FIG. 27. Linewidth of the quantum beat of *Figure 26* versus distance from the nozzle. The linewidths were determined as mentioned in the text.

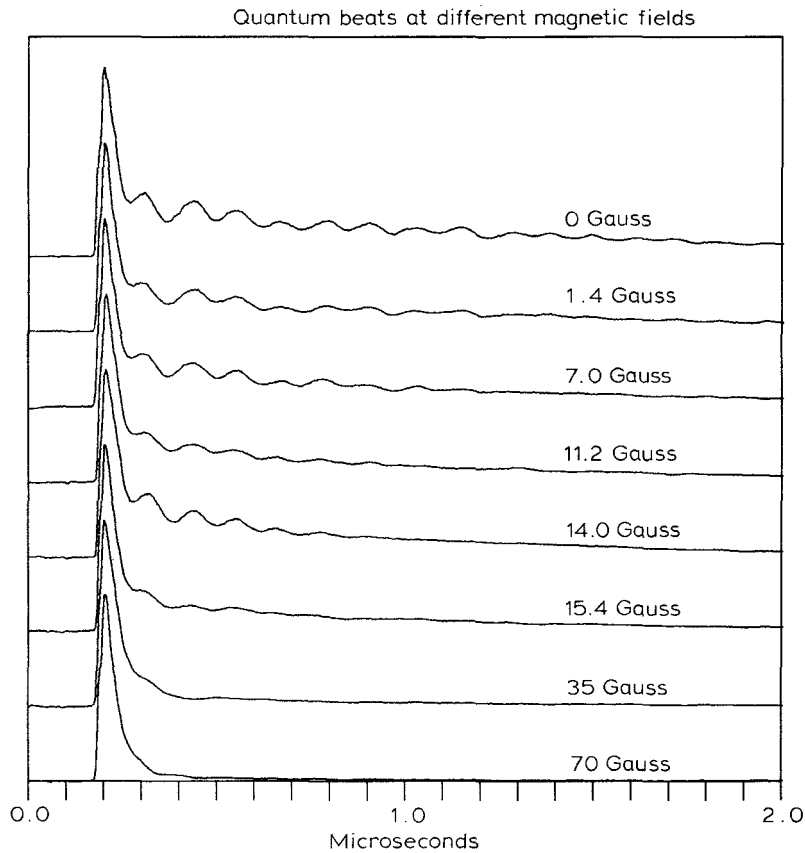

FIG. 28. Quantum beats of *Figure 25* at different magnetic fields, which were oriented along the direction of propagation of the laser.

conservation of angular momentum and of rotational interactions in an isolated molecule undergoing radiationless transition. Later Novak and Rice (1979, 1980) extended this analysis, provided a treatment of the effect of Coriolis coupling on internal conversion in rotating molecules and investigated the effects on the rate of intersystem crossing of rotational state dependence of spin–orbit coupling, of differences in moments of inertia between the coupled electronic states, of Coriolis coupling, and of vibration–rotation interaction in the initial state (Novak *et al.*, 1980).

Recently Henke *et al.* (1981b) have extended the theory of Howard and Schlag, and Novak and Rice to study the following effects.

1. The effect of rotational energy gap on the SRVL NR rate constant.
2. The effect of the vibration–rotation coupling through the change of moment of inertia.
3. The effect of the vibration–rotation coupling through the Coriolis interaction.
4. The dynamical effect of intramolecular vibrational dephasing (i.e., the damping effect) (that is, the small or intermediate molecule case).
5. The electric field effect on the SRVL NR rate.

They have applied their theoretical results to interpret the recent experimental data of SRVL lifetimes of formaldehyde and pyrazine; the agreement between theory and experiment is found to be reasonably good. It is believed that the theoretical method can now be used for analysing the experimental results of SRVL NR rate measurements. In this paper, the main results of the theory will be presented.

For the present discussion, only bound states will be considered and for convenience we restrict ourselves to symmetric top molecules. However, the theory to be presented in this paper can be generalized to treat other types of molecules. The total angular momentum due to molecular rotation of a symmetric top molecule is characterized by the quantum number J and its projection on the symmetric top axis is denoted by K. In large, symmetric top molecules they are usually good quantum numbers.

Let N represent the total angular momentum including spin S and P, the projection of N on the symmetric top axis. For the case in which the quantum numbers J, K, N and S are good, they characterize a state by $|\alpha\ SNJK\rangle$ where α represents all other quantum numbers. This set of good quantum numbers implies a Hund's case (b) angular momentum coupling scheme, i.e.,

$$\vec{J} = \vec{N} - \vec{S} \tag{6}$$

Note that J and not N is used to denote the total angular momentum excluding spin.

Now if the electron spin is strongly coupled to the molecular frame, Hund's case (a) generally applies. In this coupling scheme, the quantum numbers S, S_z, N and P are good and a molecular state is described by the wavefunction $|\alpha\ SS_z\ NP\rangle$. We note that for high rotational quantum numbers J, no molecule is well described in Hund's case (a) and that in the solid phase, $\hat{S}$ is generally the only operator responsible for molecular angular momentum and thus the quantum numbers S and S_z will be the good quantum numbers.

It should be noted that the above discussion has not included the nuclear spin operator $\vec{I}$, which we can add to $\vec{N}$ to produce $\vec{F}$.

Internal conversion

For a singlet state, since $S = 0$, Eq. (6) reduces to

$$\vec{N} = \vec{J} \tag{7}$$

It follows that $N = J$ and $K = P$. For internal conversion (IC) between any two singlet states, the rate constant of a SRVL ($bv\ JKM$) can, in general, be expressed as

$$W_{bvJKM} = \frac{2\pi}{\hbar} \sum_{v'J'K'M'} |\langle av'J'K'M'|\hat{H}'|bvJKM\rangle^2 \times D(E_{av'J'K'M'} - E_{bvJKM}) \tag{8}$$

where D is a function of energy difference and width of the involved states, and $\hat{H}'$ represents the perturbation that induces the radiationless transition and M represents the magnetic quantum number along the space-fixed Z-axis. Depending on whether we are concerned with the symmetric rotor or asymmetric rotor, the rotational quantum number K will be different. In general, in the absence of an external field one can only observe $W_{bvJK'}$ i.e.

$$W_{bvJK} = \frac{1}{2J+1} \sum_{M} W_{bvJKM} \tag{9}$$

In a large molecule, one can usually make the approximation

$$W_{bvJKM} = \frac{2\pi}{\hbar} \sum_{v'J'K'M'} |\langle av'J'K'M'|\hat{H}'|bvJKM\rangle^2 + \delta(E_{av'J'K'M'} - E_{bvJKM}) \quad (10)$$

where $\delta(x)$ is the delta function. In the absence of an external field, E_{bvJKM} becomes E_{bvJK}.

The matrix elements involved in Eq. (8) depend on the choice of interaction operator $\hat{H}'$ or alternatively, on the choice of representation of the zeroth order wavefunctions. For large molecules, it is generally agreed that a Born–Oppenheimer (BO) basis set with spin uncoupled from the molecular frame is the most appropriate. Transitions between zeroth order states can be induced by $\hat{T}_N$ (or $\hat{H}'_{\mathrm{BO}}$, the so-called BO coupling), the nuclear kinetic energy operator.

No vibration–rotation interaction

First we consider the case in which the vibration–rotation interaction can be ignored. In this case, using the adiabatic approximation we have

$$|bvJKM> = \Phi_b \oplus_{bv} Y_{JKM} \quad (11)$$

$$|av'J'K'M'> = \Phi_a \oplus_{av'} Y_{J'K'M'} \quad (12)$$

where Φ_a, Φ_b are electronic wavefunctions, $\oplus_{bv}, \oplus_{av'}$, vibrational wavefunctions and Y_{JKM}, $Y_{J'K'M'}$, rotational wavefunctions. If $\hat{H}'_{\mathrm{BO}}$ which is responsible for internal conversion does not involve the molecular rotation, then

$$\begin{aligned}\langle av'J'K'M'|\hat{H}'|bvJKM\rangle &= \langle \Phi_a \oplus_{av'}|\hat{H}'_{\mathrm{BO}}|\Phi_b \oplus_{bv}\rangle \langle Y_{J'K'M'}|Y_{JKM}\rangle \\ &= \langle \Phi_a \oplus_{av'}|\hat{H}'_{\mathrm{BO}}|\Phi_b \oplus_{bv}\rangle \, \delta_{JJ'} \, \delta_{KK'} \, \delta_{MM'} \end{aligned} \quad (13)$$

That is, we obtain the selection rules $\Delta J = 0$, $\Delta K = 0$, $\Delta M = 0$.
Substituting Eq. (13) into Eq. (8) yields

$$W_{bvJK} = \frac{2\pi}{\hbar} \sum_{v'} |\langle \Phi_a \oplus_{av'}|\hat{H}'_{\mathrm{BO}}|\Phi_b \oplus_{bv}\rangle|^2 \times \delta(E_{av'J'K'} - E_{bvJK}) \quad (14)$$

for the large molecule case. Here it is assumed that no external field is present. From Eq. (14) we can see that the rotational dependence of the SRVL NR rate constant is through the energy gap $E_{av'J'K'} - E_{bvJK}$ which in turn depends on the difference in moments of inertia between the two electronic states. This effect was first pointed out by Howard and Schlag (1978b).

Using the relation

$$\langle \Phi_a \oplus_{av'}|\hat{H}'_{\mathrm{BO}}|\Phi_b \oplus_{bv}\rangle = -\hbar^2 \sum_i \langle \Phi_a \oplus_{av'}| \frac{\partial \Phi_b}{\partial Q_i} \frac{\partial \oplus_{bv}}{\partial Q_i}\rangle = \sum_i \langle \oplus_{av'}|R_i(ab)| \frac{\partial \oplus_{bv}}{\partial Q_i}\rangle \quad (15)$$

where

$$\mathrm{R}_i(ab) = -\hbar^2 \langle \Phi_a| \frac{\partial \Phi_b}{\partial Q_i}\rangle,$$

Eq. (14) becomes

$$W_{bvJK} = \frac{2\pi}{\hbar} \sum_{v'} \left| \sum_{i} \langle \oplus_{av'} | R_i(ab) | \frac{\partial \oplus_{bv}}{\partial Q_i} \rangle \right|^2 \delta(E_{av'J'K'} - E_{bvJK}) \tag{16}$$

This equation is quite general and can be used for actual numerical calculation. However, it is often convenient to have approximate analytical expressions that can be used to interpret the experimental results. For this purpose, the displaced-oscillator model and the Condon approximation are commonly used. In this case, we find (Henke *et al.*, 1982b; Lin, 1973)

$$W_{bvJK} = \sum_{i} \frac{|C_i(ab)|^2}{\hbar^2} \exp(-\tfrac{1}{2} \sum_{j} \Delta_j^2) \int_{-\infty}^{\infty} dt \exp[\tfrac{1}{2} \times \sum_{j} \Delta_j^2 e^{it\omega_j} + it(\omega_{aJK,bJK} + \omega_i)] f_{bv}(t) \tag{17}$$

where

$$\omega_{aJK,bJK} = \omega_{ab} + \omega_{aJK}^{(\mathrm{rot})} - \omega_{bJK}^{(\mathrm{rot})},$$

Δ_j is the dimensionless normal coordinate displacement and

$$f_{bv}(t) = [(v_i + 1) + v_i e^{-2it\omega_i}] \sum_{n_1=0}^{v_1} \cdots \sum_{n_N=0}^{v_N} \prod_{j} \frac{v_j! \, \Delta_j^{2n_j}}{(v_j - n_j)! \, (n_j!)^2} \times (\cos \omega_j t - 1)^{n_j} \tag{18}$$

Here

$$C_i(ab) = \sqrt{\frac{\omega_i}{2\hbar}} R_i(ab).$$

To evaluate the integral in Eq. (17) the saddle-point method can be used. In this case, we obtain (Henke *et al.*, 1982b)

$$W_{bvJK} = \sum_{i} W_{b\,000}(i) f_{bvJK}(i) \tag{19}$$

and

$$\frac{W_{bvJK}}{W_{bv\,000}} = \exp(it_i^* \, \omega_{aJK,\,bJK}^{(\mathrm{rot})}) \tag{20}$$

Equation (20) describes the rotational dependence of the NR rate constant in a given vibronic manifold: it depends only on the rotational energy difference $\omega_{aJK,bJK}^{(\mathrm{rot})}$. Notice that t_i^* is determined by

$$\omega_{ba} - \omega_i = \sum_{j} \tfrac{1}{2} \Delta_j^2 \, \omega_j \exp(it_i^* \, \omega_j) \tag{21}$$

To demonstrate the rotational dependence of the SRVL NR rate based on the use of the displaced oscillator model the numerical calculation will be performed for the following cases. The first case is

$$\omega_j = 1000 \text{ cm}^{-1}, \qquad \Delta_j^2 = 0.1, \qquad \omega_{ba} = 28\,000 \text{ cm}^{-1} \tag{22}$$

and the total number of accepting modes is six. For the moments of inertia we use:

Ground state:

$$\tilde{A} = 9.405, \qquad \tilde{B} = \tilde{C} = 1.215 \text{ cm}^{-1} \tag{a}$$

Excited state:

$$\tilde{A} = 8.7518, \qquad \tilde{B} = \tilde{C} = 1.068 \text{ cm}^{-1} \tag{b}$$

The second case is to use the following moments of inertia:

Ground state:

$$\tilde{A} = \tilde{B} = 0.1896 \text{ cm}^{-1}, \qquad \tilde{C} = \frac{\tilde{B}}{2} \tag{c}$$

Excited state:

$$\tilde{A} = \tilde{B} = 0.1813 \text{ cm}^{-1}, \qquad \tilde{C} = \frac{\tilde{B}}{2} \tag{d}$$

Other physical constants are the same as the first case except for the number of accepting modes which is changed to 30. The numerical results are shown in *Figure 29*. To show the effect of the coupling strength (determined by the magnitude of Δ_j^2) on the SRVL NR rate constant, we repeat the above calculations by changing Δ_j^2 from 0.1 to 0.05; the results are also shown in *Figure 29* (Henke *et al.*, 1982b).

Needless to say, the theoretical results presented above can be used for not only the rotational effect but also the vibronic effect on the NR rate constant, i.e., the vJK dependence of the NR rate constant (Heller *et al.*, 1972). In the case where the vibration–rotation interaction is negligible and $\hat{H}'_{BO}$ that is used does not depend on molecular rotation (because the Coriolis coupling in $\hat{T}_N$ can also induce a radiationless transition), the selection rules $\Delta J = 0$, $\Delta K = 0$ and $\Delta M = 0$ hold, and the rotational dependence of the SRVL NR rate in a given vibronic manifold is only through the rotational energy gap $\omega^{(\text{rot})}_{aJK,bJK}$ for a symmetric rotor. Furthermore, from Eqs. (20) and (21), one can predict that the rotational (JK) dependence of the NR rate constant is approximately the same regardless of the vibronic manifolds (bV). This provides a way to analyse the experimental data of the SRVL NR rate constant W_{bvJK}.

Notice that in *Figure 29a* the maximum J value is 15, while in *Figure 29b* the maximum J value is 80. From *Figure 29a* and *b* we can see that the rotational dependence of SRVL NR rates is significant, the weaker coupling case (smaller Δ_j^2 values) shows a stronger rotational dependence and the smaller the rotational constant changes between the two electronic states, the smaller the rotational effect on SRVL NR rates.

It should be noted that the numerical calculation presented in this section is based on the use of Eq. (17) in which the changes in normal frequency between the two electronic states are not taken into account; for practical interpretation of experimental results this effect may not be negligible.

In the above discussion, we have treated only the IC between singlet states. However, the same results should apply to IC of spin states of other multiplicities provided that $\hat{H}'$ in Eq. (8) does not involve spin operators.

Effect of vibration–rotation coupling through the change of moments of inertia

Notice that the rotational Hamiltonian of a symmetric rotor can be expressed as (Kroto, 1975):

$$\hat{H}_r = B(Q)\hat{J}^2 + \Delta B(Q)\hat{J}_z^2 \tag{23}$$

where $\Delta B(Q)$ may be positive or negative depending on whether the rotor is prolate or oblate. The moments of inertia are in general a function of normal coordinates.

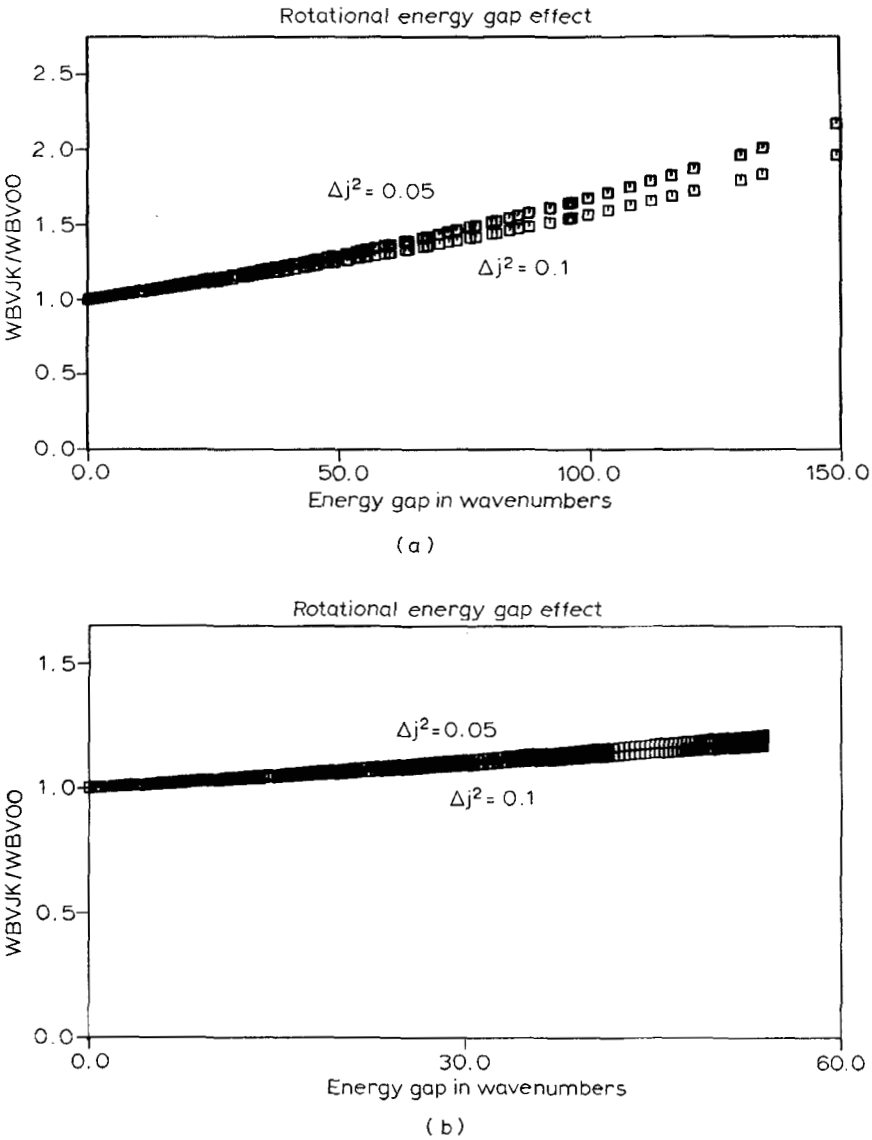

FIG. 29. (a) The effect of rotational energy gap. Parameters for the calculation were (cm^{-1}): lower curve: $A = 9.045$, $B = C = 1.215$; excited state: $A = 8.7518$, $B = C = 1.068$; number of accepting modes: 6; $\Delta_j^2 = 0.1$; $J_{max} = 15$; upper curve: same parameters but $\Delta_j^2 = 0.05$. (b) Parameters: lower curve: $A = B = 0.1896$, $C = B/2$; excited state $A = B = 0.1813$, $C = B/2$; number of accepting modes: 30; $\Delta_j^2 = 0.1$; $J_{max} = 80$; upper curve: same parameters, but $\Delta_j^2 = 0.05$.

Expanding $B(Q)$ and $\Delta B(Q)$ in power series of normal coordinates Q_j yields

$$\hat{H}_r = \hat{H}_r^0 + \hat{H}_r' \tag{24}$$

where

$$\hat{H}_r^0 = B(0)\hat{J}^2 + \Delta B(0)\hat{J}_z^2 \tag{25}$$

and

$$\hat{H}_r' = \sum_j Q_j \left(\frac{\partial B}{\partial Q_j} \hat{J}^2 + \frac{\partial \Delta B}{\partial Q_j} \hat{J}_z^2 \right) + \dots \tag{26}$$

$\hat{H}_r'$ represents the vibration–rotation coupling through the changes of moments of inertia.

If the internal conversion is induced by a perturbation that does not involve the molecular rotation, then the effect of $\hat{H}_r'$ can easily be included in the calculation of the SRVL NR rate W_{bvJK}. Due to the normal coordinate dependence of $\hat{H}_r'$, the vibrational wavefunction will be affected. For example, if the molecular vibration is harmonic, then the linear dependence of $\hat{H}_r'$ on normal coordinates will affect the vibrational wavefunction by shifting the normal coordinate,

$$Q_j(JK) = Q_j + \Delta Q_j(JK) \tag{27}$$

where

$$\Delta Q_j(JK) = \frac{1}{\omega_j^2} \left[\frac{\partial B}{\partial Q_j} J(J+1) + \frac{\partial \Delta B}{\partial Q_j} K^2 \right] \hbar^2 \tag{28}$$

represents the normal coordinate shift induced by $\hat{H}_r'$. The resulting vibrational wavefunction is still harmonic with Q_j being replaced by $Q_j(JK)$ given by Eq. (27). To show this effect on the SRVL NR rate explicitly, let us consider the displaced oscillator model; in the Condon approximation and for a symmetric rotor, we find (Henke *et al.*, 1982b)

$$W_{bvJK} = \sum_i \frac{|C_i(ab)|^2}{\hbar^2} \exp[-\sum_j \tfrac{1}{2}\Delta_j(JK)^2] \int_{-\infty}^{\infty} dt \exp[\tfrac{1}{2} \times \sum_j \Delta_j(JK)^2 e^{it\omega_j} + it(\omega_{ab} + \omega_i)] f_{bvJK}(t) \tag{29}$$

where

$$f_{bvJK}(t) = \exp(it\omega_{aJK,bJK}^{(\mathrm{rot})}) [(v_i + 1) + v_i e^{-2it\omega_i}] \times \sum_{n_1=0}^{v_1} \dots \sum_{n_N=0}^{v_N} \prod_j \frac{v_j! \, \Delta_j(JK)^{2n_j}}{(v_j - n_j)! \, (n_j!)^2} (\cos \omega_j t - 1)^{n_j} \tag{30}$$

$$\Delta_j(JK) = \Delta_j + \frac{1}{\sqrt{\hbar}\, \omega_j^3} \Delta a_{jJK} \tag{31}$$

and

$$\Delta a_{jJK} = \hbar^2 \left[\left(\frac{\partial B}{\partial Q_j} \right)_a - \left(\frac{\partial B}{\partial Q_j} \right)_b \right] J(J+1) + \hbar^2 \left[\left(\frac{\partial \Delta B}{\partial Q_j} \right)_a - \left(\frac{\partial \Delta B}{\partial Q_j} \right)_b \right] K^2 \tag{32}$$

For the purpose of numerical calculation to see the effect of vibration–rotation coupling through the change of moments of inertia on the SRVL NR rate, we consider the case

that there is only one promoting mode and $v = 0$, the lowest vibronic level, and again use the model described in the previous section (*see* Eqs. (a) to (d)). In addition, we need to specify Δa_{jJK} or equivalently,

$$\frac{\Delta a_{jJK}}{\sqrt{\hbar\,\omega_j^3}}\,\Delta_j = \alpha_j J(J+1) + \beta_j K^2 \tag{33}$$

Here we shall for convenience assume that α_j and β_j are the same for all the modes and $\alpha_j = \beta_j = 0.25 \times 10^{-5}$.

The numerical results are shown in *Figure 30*. Now due to the vibration–rotation coupling, the SRVL NR rate does not vary monotonically in a single-valued way with the rotational energy gap as shown in *Figure 29*. This type of the vibration–rotation coupling effect depends on the changes of moments of inertia with respect to normal coordinates between the two electronic states involved (*see* for example Δa_{jJK} in Eq. (33). Depending on the magnitude of Δa_{jJK}, this effect on the SRVL NR rate can be significant. Depending on the signs of Δa_{jJK} the contribution from the effect of vibration–rotation coupling through the changes of moments of inertia can increase or decrease the SRVL NR rates with the increasing (J, K) values. Furthermore, because of the Δa_{jJK} involvement in $\Delta_j(JK)$ (*see* for example Eqs. (29) and (30) this effect may become stronger at higher vibronic levels (i.e. larger v_j values).

Effect of Coriolis coupling

Notice that the Coriolis interaction can in general be expressed as (Kroto, 1975):

$$\hat{H}'_{\mathrm{Cor}} = -\sum_{\alpha} \frac{\hat{M}_\alpha \hat{m}_\alpha}{I_\alpha} = -\sum_{\alpha} \sum_{k} \sum_{l} \frac{\hat{M}_\alpha}{2I_\alpha}\,\zeta_{kl}^{(\alpha)}\,(Q_l \hat{p}_k - Q_k \hat{p}_l) \tag{34}$$

where I_α represents moments of inertia, $\hat{M}_\alpha$ rotational angular momentum operators, $\hat{m}_\alpha$ vibrational angular momentum operators and $\zeta_{kl}^{(\alpha)}$ Coriolis coupling constants.

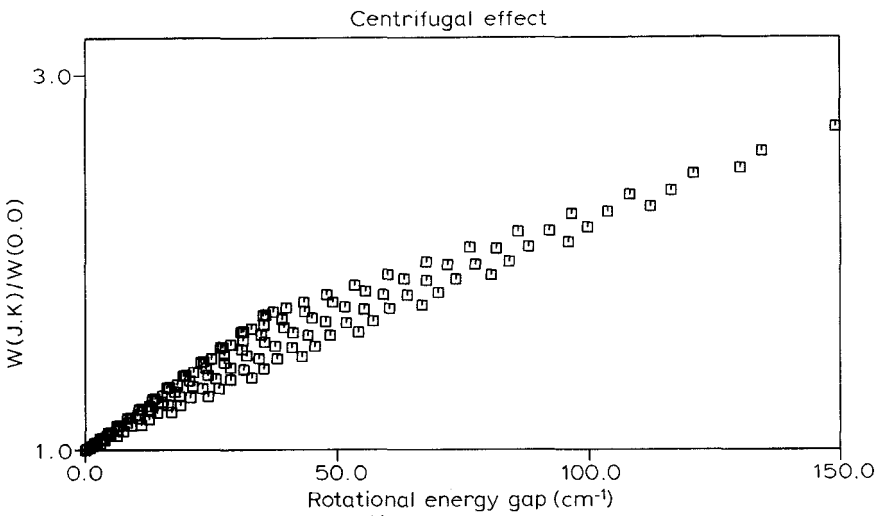

FIG. 30. Effect of vibration–rotation coupling through the change of moment of inertia. (*See* text for parameters for the calculation.)

To treat the effect of Coriolis coupling on the NR rate constant we first consider the case of the Coriolis coupling that involves only two degenerate vibrational modes and for simplicity assume that the Coriolis interaction takes the form

$$\hat{H}'_r = -\frac{\hat{M}_z \hat{m}_z}{I_z} = -\frac{\hat{M}_z \zeta_{kl}^{(z)}}{I_z} (Q_l \hat{p}_k - Q \hat{p}_l) \tag{35}$$

i.e., only z-components of vibrational and rotational angular momenta are coupled.

For the case that the rotational quantum number J remains unchanged by the Coriolis interaction and for low vibrational quantum numbers ($v_k = 0$, $v_l = 1$) one can use the perturbation method if the rotational energy separation is larger than the magnitude of the Coriolis interaction (Henke *et al.*, 1981b). Next we discuss the effect of $\hat{H}'_{\text{Cor}}$ on the final states (i.e., the dynamical effect) in the SRVL NR rates; this effect was first treated by Novak and Rice (1980) for ISC. One obtains for IC (Henke *et al.*, 1982b)

$$W_{bvJK} = \sum_i \frac{|C_i(ab)|^2}{\hbar^2} \exp(-\tfrac{1}{2} \sum_j \Delta_j^2) \int_{-\infty}^{\infty} dt \exp[\tfrac{1}{2} \sum_j \Delta_j^2 \exp(it\omega_j) + it(\omega_{aJK,bJK} + \omega_i)]$$
$$\exp\left[-K^2 \sum_j \sum_k{}' \left| \frac{\Delta_j \zeta_{kj}^{(z)}}{4I_z} \left(\sqrt{\frac{\omega_j}{\omega_k}} + \sqrt{\frac{\omega_k}{\omega_j}} \right) \frac{(e^{it\omega_j} - e^{it\omega_k})}{\omega_j - \omega_k} \right|^2 \right] \tag{36}$$

Here, for simplicity, we have only treated the case of the lowest vibronic level. As can be seen from Eq. (36), the effect of the Coriolis coupling is significant when the vibrational modes involved in $\hat{H}'_{\text{Cor}}$ are degenerate. For example, if only degenerate Q_k and Q_l are involved in $\hat{H}'_{\text{Cor}}$ as given by Eq. (35), Eq (36) becomes

$$W_{boJK} = \sum_i \frac{|C_i(ab)|^2}{\hbar^2} \exp(-\tfrac{1}{2} \sum_j \Delta_j^2) \int_{-\infty}^{\infty} dt \exp[\tfrac{1}{2} \sum_j \Delta_j^2 \exp(it\omega_j) + it(\omega_{aJK,bJK} + \omega_i)]$$
$$\exp\left[-K^2 \left| \frac{\Delta_k \zeta_{kl}^{(z)}}{2I_z} (it) \right|^2 \right] \tag{37}$$

The correction factor due to the Coriolis coupling $F_{i,\text{Cor}}$ can be evaluated by using the saddle-point method, (Henke *et al.*,1981b).

$$F_{i,\text{Cor}} = \exp\left[-K^2 \left| \frac{\Delta_k \zeta_{kl}^{(z)}}{2 I_z} (it_i^*) \right|^2 \right] \tag{38}$$

where the saddle-point value t_i^* is determined by Eq. (21).

From the above discussion of the Coriolis coupling effect, for a given J value the SRVL NR rate decreases with increasing values of K^2. Notice that the effect of $\hat{H}'_{\text{Cor}}$ on SRVL NR rates for higher vibronic levels and for the case of $\zeta_{kl}^{(x)} \neq 0$ and/or $\zeta_{kl}^{(y)} \neq 0$ has not been studied.

Application

In the previous sections the theoretical treatment of the SRVL NR rate dependence on rotation was given. Here the results are discussed in view of recent experimental results.

In 4_0^1 and 4_0^3 bands of formaldehyde it was found, that the lifetimes generally decrease with increasing rotation as shown in the experimental section. From the theoretical treatment of the SRVL NR rates (i.e. ignoring the vibration–rotation interaction) it was shown that the SRVL NR rates should depend only on the rotational energy gap, $\omega^{(\mathrm{rot})}_{aJK,bJK}$ (*see* Eq. (17) or Eq. (20)). As can be seen from *Figure 29a*, this effect is significant. The decay rate for the maximum value of the rotational quantum number in the calculation is approximately twice as fast as for the lowest rotational quantum number. But it was shown that the SRVL lifetimes of H_2CO do not just depend on the rotational energy gap. The effect of the rotational energy gap is small for the rotational levels which were observed in the jet experiments. Therefore the centrifugal effect, or the vibration–rotation coupling due to change of moments of inertia is considered to explain the lifetimes. In *Figure 31* the 4_0^3 experimental decay rates are compared to the theoretical model. The calculation is based on Eq. (29) and the application of the saddle-point method, i.e., $f_{bvJK}(t^*)$ for the ν_4 mode. For this purpose, from Eq. (29) we

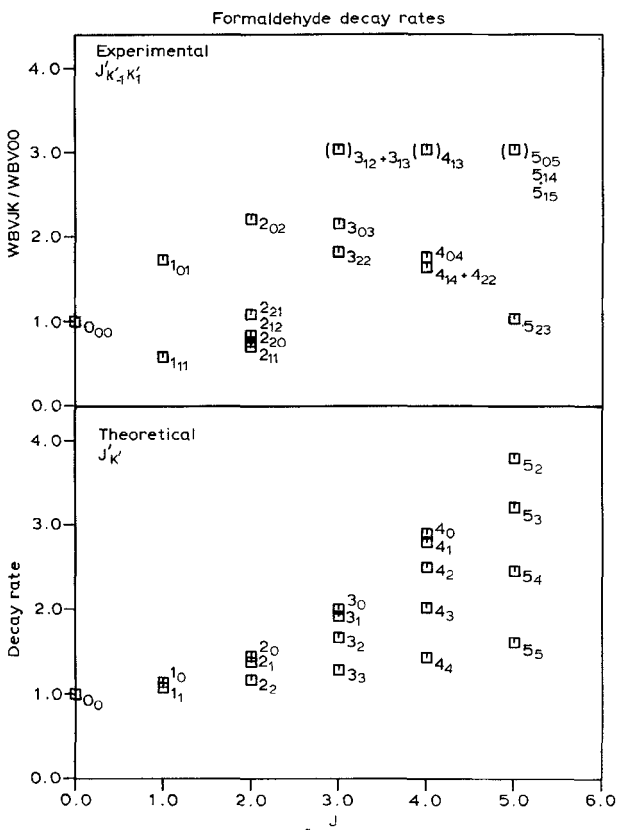

FIG. 31. Comparison between experimental (upper trace) and calculated SRVL NR rate constants for the 4^3 band of formaldehyde. (From Henke *et al.*, 1982b.)

can see that it is necessary to know Δ_4 and Δa_{4JK} (*see* Eq. (33)). Δ_4 can be estimated from the vibrational effect alone. The average decay rates increase by a factor of roughly 30 if one compares the 4^1 and 4^3 vibrational levels. From this we obtain $|\Delta_4| = 0.05$. Within the 4^3 level the decay rates of rotational levels vary as shown in *Figure 31*. To interpret this rotational dependence, $\alpha_4 = 1.00 \times 10^{-4}$ and $\beta_4 = -1.00 \times 10^{-4}$ have been chosen. Experimental and theoretical results are compared in *Figure 31*. As can been seen from this figure the 4^3 decay rates can be reasonably explained.

Figure 32 shows the experimental SRVL decay rates of the 2^24^1 level of formaldehyde. In this case the decay rates increase with K for each value of J; this can be explained by a different sign of β_2 in Eq. (33). The input parameters for the calculated decay rates are $|\Delta_2| = 0.300$, $\alpha_2 = 1.00 \times 10^{-4}$ and $\beta_2 = 2.00 \times 10^{-4}$. In this case, the agreement between theory and experiment is again reasonable. It should be noted that the K dependence in the 2^24^1 band is reversed compared to that in the 4^3 band. Another explanation to that presented above (i.e. the different signs of β_j in the two different bands) is that there exists a Coriolis coupling in the 4^3 band. The interacting level is the 6^1 state as shown in the experimental section. From Eq. (37) one

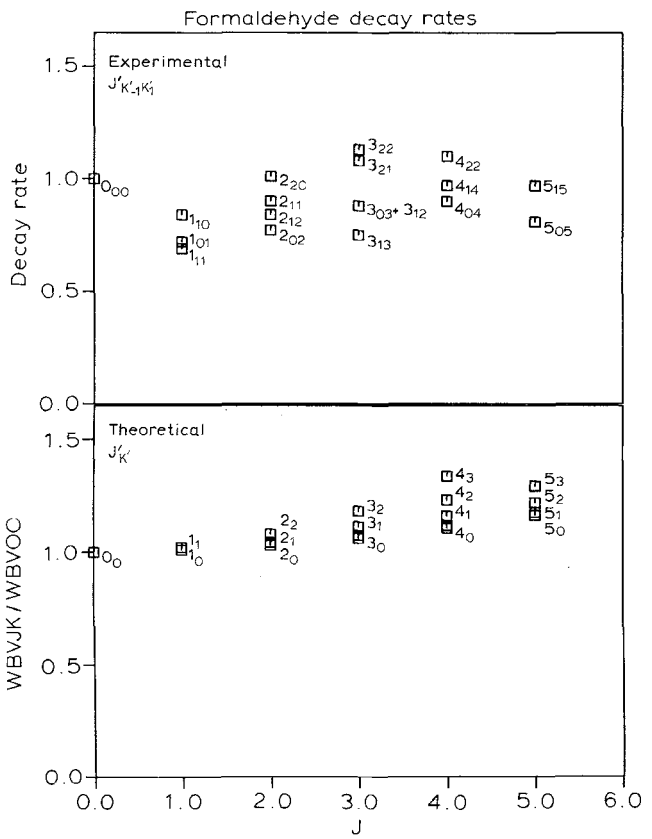

FIG. 32. Comparison between experimental (upper trace) and calculated SRVL NR rate constants for the 2^24^1 band of formaldehyde. Experimental values are taken from Selzle and Schlag (1979).

can see that in this case the SRVL NR rate is expected to decrease with increasing K, which is the case for the 4^3 decay rates. A crude estimation of Δ_j in H_2CO based on the internal coordinates and equilibrium nuclear geometries in the S_0 and S_1 electronic states shows that in fact Δ_2 is larger than Δ_4 as predicted above.

From *Figures 31 and 32* we can see that the discrepancy between experiment and theory still exists. This may be in part due to the fact that formaldehyde is not a symmetric rotor and in part due to the use of the conventional Condon approximation and the displaced harmonic oscillator model. To fully analyse the SRVL lifetime data of H_2CO, it requires to take into account explicitly the interaction between the inversion mode (ν_4 mode) of the $^1A_2$ state and the $^1A_1$ state with rotation and other vibrational modes. A promising treatment of this type of interaction has been given (Moule and Rao, 1973).

For an intermediate size or small molecule the damping effect (or effect of vibrational dephasing) plays an important role in the calculation of the collision-free NR rate constant. In this case, the energy matching is only required to within the level width. That is, in this case, W_{bvJK} (in the absence of an external field) should be calculated by using Eq. (8). This case has been treated by Henke *et al.* (1982b) by assuming that the damping constants vary linearly with the vibrational quantum numbers.

The effect of an electric field on SRVL lifetimes of formaldehyde has been measured by Weisshaar and Moore (1980) and is found to be significant in the field strength range 0–4.6 kV/cm. The electric field effect on radiative and NR rates of large molecules (Lin *et al.*, 1980; Strek, 1978; Lin, 1975) and SRVL NR rates of small or intermediate-size molecules (Henke *et al.*, 1981) has been treated theoretically. It has been shown that the electric field can induce NR transitions, and can affect NR rates through its effect on wavefunctions and energy gap involved in the Lorentzian; i.e. the electric field can shift the energy matching out of resonance which may be quite important for small or intermediate size molecules.

Intersystem crossing

As discussed in the previous section, for a great number of polyatomic molecules, the quantum numbers J, K, N and S are good quantum numbers; they can be used to characterize a single rovibronic state $|bvSNJK\rangle$ (i.e., Hund's case (b)). The SRVL NR rate for the state $(bvSNJK)$ can then be expressed as:

$$W_{bvSNJK} = \frac{2\pi}{\hbar} \sum_{v'N'J'K'} |\langle av'S'N'J'K'|\hat{H}'|bvSNJK\rangle|^2 D(E_{bvSNJK} - E_{av'S'N'J'K'}) \quad (39)$$

where $S \neq S'$. For ISC, the spin–orbit coupling $\hat{H}_{SO}$ or vibronic spin–orbit coupling is commonly used to calculate the NR rates (Hallin and Merer, 1977; Henry and Siebrand, 1971; Lin, 1966).

To calculate the matrix elements involved in Eq. (39) it is often convenient to use a basis set in Hund's case (a). The case (b) wavefunctions can be expanded in terms of the case a wavefunctions,

$$|av'S'N'J'K'\rangle = \sum_{PS_z} (S' - S'_zN'P'|S'N'J'K')|av'S' - S'_zN'P'\rangle \quad (40)$$

where $(S' - S'_zN'P'|S'N'J'K')$ represents the Clebsch–Cordon coefficient which is

related to the Wigner 3 − J symbol by

$$(S' - S'_z N' P' | S' N' J' K') = (-1)^{N' - S' - K'} (2J' + 1)^{\frac{1}{2}} \begin{pmatrix} N' & J' & S' \\ P' & -K' & -S'_z \end{pmatrix} \tag{41}$$

Substituting Eq. (40) into Eq. (41) yields

$$|av'S''N'J'K'\rangle = \sum_{P'S'_z} (-1)^{N' - S' - K'} (2J + 1) \begin{pmatrix} N' & J' & S' \\ P' & -K' & -S'_z \end{pmatrix} |av'S' - S'_z N' P'\rangle \tag{42}$$

No vibration–rotation interaction

In this case, angular momentum must be conserved for all internal degrees of freedom of the molecule in bound states of isolated molecules; i.e., no internal process can alter N, the total angular momentum including spin and $\vec{P}$, the projection of $\vec{N}$ on the symmetric top axis. In other words, we have the selection rules $\Delta N = 0$ and $\Delta P = 0$ for ISC and IC.

For most ISC's observed in experiments the singlet state is involved in either the initial state or the final state. Notice that the singlet wavefunctions are the same in Hund's case (a) and (b) since $S = 0$. In this case, the matrix element in Eq. (39) becomes

$$\langle av'S'N'J'K' | \hat{H}' | bvSNJK\rangle = \sum_{P'S'_z} (-1)^{N' - S' - K'} (2J' + 1)^{1/2} \begin{pmatrix} N' & J' & S' \\ P' & -K' & -S'_z \end{pmatrix} \langle av'S' - S'_z N' P' | \hat{H}'_{SO} | bv00JK\rangle \tag{43}$$

Using the selection rules of $\Delta N = 0$ and $\Delta P = 0$, we obtain $N' = J$ and $P' = K$. It follows that

$$\langle av'S'N'J'K' | \hat{H}' | bvSNJK\rangle = \sum_{S'_z} (-1)^{J - S' - K'} (2J' + 1)^{1/2} \begin{pmatrix} J & J' & S' \\ K & -K' & -S_z \end{pmatrix} \langle av'S' - S'_z | \hat{H}'_{SO} | bv00\rangle \tag{44}$$

Rotation selection rules can be obtained from the Wigner 3–J symbol involved in Eq. (44),

i.e.,

$$|J - J'| \leq S' \leq J + J' \tag{45}$$

and

$$K = K' + S'_z \tag{46}$$

For single–triplet transitions, we have $S' = 1$ and (Howard and Schlag, 1978b, 1980)

$$\Delta J = \pm 1,0; \qquad \Delta K = \pm 1,0 \tag{47}$$

From Eq. (39) we note that if the Franck–Condon factors to all final vibrational states

are equal and if one can neglect the rotational energy gap dependence, then the following sum rule applies:

$$\sum_{J'K'} (2J' + 1) \begin{pmatrix} J & J' & S' \\ K & -K' & -S'_z \end{pmatrix}^2 = 1 \tag{48}$$

Thus if the Franck–Condon weighted density of states is constant in the energy region scanned by the rotational states, then the ISC rate constant will be independent of rotational state selection (Howard and Schlag, 1978b, 1980).

Effect of vibration–rotation coupling through the change of moments of inertia

As can be seen from the discussion of the previous sections, in the absence of interaction between the rotational and vibrational degrees of freedom the rotational effect on SRVL NR rates mainly comes through the rotational energy gap. To treat the effect of vibration–rotation coupling on SRVL NR rates, it is often convenient to use the correlation-function form of W_{bvSNJK} (Fischer, 1970)

$$W_{bvSNJK} = \frac{1}{\hbar^2} \int_{-\infty}^{\infty} dt \, \langle bvSNJK | \hat{H}'(0) \hat{H}'(t) | bvSNJK \rangle \tag{49}$$

where

$$\hat{H}'(t) = \exp\left(\frac{it}{\hbar} \hat{H}_a\right) \hat{H}' \exp\left(-\frac{it}{\hbar} \hat{H}_b\right) \tag{50}$$

and $\hat{H}_a$ and $\hat{H}_b$ represent the rovibronic Hamiltonians of the a electronic state and b electronic state, respectively. Using Eq. (49) it is easy to choose or change the basis set of the final electronic state.

We now consider the effect of the change of moments of inertia on SRVL ISC rates. In this case, the Hamiltonian for the vibration-rotation coupling is given on page 76. To show this effect on the SRVL NR explicity, we treat the displaced oscillator model. In the Condon approximation we find for the case in which the initial state is singlet,

$$W_{bv00JK} = W_{bvSS_zJK} = \frac{1}{\hbar^2} |C(0S')|^2 \exp\left[-\sum_j \tfrac{1}{2}\Delta_j(JK)^2\right] \times \int_{-\infty}^{\infty} dt \exp\left[\tfrac{1}{2}\sum_j \Delta_j(JK)^2 e^{it\omega_j} + it\omega_{aJK,bJK}\right] f^{(t)}_{bvJK} \tag{51}$$

where $\Delta_j(JK)$ and $f^{(t)}_{bvJK}$ are defined on page 76, and

$$|C(0S')|^2 = \sum_{S'_z} |\langle b00 | \hat{H}'_{SO} | aS'S'_z \rangle|^2 \tag{52}$$

Notice that $\langle b00 | \hat{H}'_{SO} | aS'S'_z \rangle$ represents the matrix element of the spin–orbit coupling.

Novak and Rice (1980) treated this vibration–rotation interaction effect on ISC first. However, they have only considered the case $v = 0$, i.e., the lowest vibronic manifold and their results are somewhat different from that given in Eq. (52) due to the different choice of adiabatic basis sets.

The SRVL NR rate W_{bv00JK} given by Eq. (52) can again be evaluated by using the saddle-point method: the results are similar to those given by Eqs. (20) and (21).

Effect of Coriolis coupling

The general expression for the Coriolis coupling is given by Eq. (34), but so far only the special case of the effect of

$$\hat{H}'_{\mathrm{Cor}} = -\sum_k \sum_l \frac{\hat{M}_z}{2I_z} \zeta_{kl}^{(z)} (Q_l \hat{P}_k - Q_k \hat{P}_l) \tag{53}$$

on ISC has been treated in the literature (Novak and Rice, 1980; Novak *et al.*, 1980). The effect of $\hat{H}'_{\mathrm{Cor}}$ in the initial state for the calculation of W_{bvSNJK} can be treated in a similar manner as that presented on page 77 for IC, but this has not been done.

The dynamical effect generated by $\hat{H}'_{\mathrm{Cor}}$ (i.e., the effect of $\hat{H}'_{\mathrm{Cor}}$ on the final states) has been studied by Novak and Rice (1980) for ISC but only for the $v = 0$ case. The $v \neq 0$ cases have not been treated. For the $v = 0$ case, W_{bv0JK} is given by

$$W_{bv0JK} = \frac{1}{\hbar^2} |C(OS')|^2 \exp(-\tfrac{1}{2}\sum_j \Delta_j^2) \int_{-\infty}^{\infty} dt \exp\left[\tfrac{1}{2}\sum_j \Delta_j^2 \exp(it\omega_j) + it\omega_{aJK,bJK} - K^2 \sum_j \sum_k{}' \left| \frac{\Delta_j \zeta_{kj}^{(z)}}{4I_z} \left(\sqrt{\frac{\omega_j}{\omega_k}} + \sqrt{\frac{\omega_k}{\omega_j}} \right) \frac{(e^{it\omega_j} e^{it\omega_k})^2}{(\omega_j - \omega_k)} \right|^2 \right] \tag{54}$$

As in the case of IC, the SRVL NR rate decreases with increasing K^2 values when the rotational energy gap is small.

Application

Recently it was found experimentally that the NR rate constants decrease proportionally to K^2 in the case of pyrazine-h_4 and pyrazine-h_2d_2 (Ter Horst *et al.*, 1981; Baba *et al.*, 1980). This is what one expects from the treatment of the vibration–rotation coupling through the change of moment of inertia (Eq. (51)) and from the Coriolis interaction (Eq. (54)). The energy gap effect is dependent on the difference between the moments of inertia of the initial and final electronic states which is small in the case of pyrazine (Innes *et al.*, 1972). The energy gap effect can therefore be ruled out. The rates in pyrazine increase by a factor of 60 if one compares the $K = 0$ and $K = 10$ rotational levels (Ter Horst, 1981). This can be explained by the vibration–rotation coupling through the change in the moments of inertia. In *Figure 33* the experimental time decay of Ter Horst *et al.* (1981) are compared to calculated decay curves based on Eq. (51). The contributions due to the different excited K rotational levels were weighted by line strength, nuclear statistical weight and Boltzmann factor (Ter Horst *et al.*, 1981).

$$I(J) = I_0 \sum_{K=-J}^{J} g_{JK} \frac{(J+1)^2 - K^2}{(J+1)} \exp(-W_{bvJK}\, t) \times \exp\left[-\frac{1}{kT} (BJ(J+1) - \tfrac{1}{2}BK^2) \right] \tag{55}$$

The input parameters in this case are $\Delta_j = 0.005$, $\alpha_j = 5 \times 10^{-7}$ and $\beta_j = 3 \times 10^{-5}$. The dependence on K^2 is significantly stronger than on J for this molecule. In this case, the rotational energy gap dependence is not very significant. From *Figure 33* we can see that the agreement between theoretical and experimental results is reasonably good.

In concluding the discussion of the theory of SRVL NR rates, we would like to point out that although the explicit expressions for SRVL NR rates are presented only for the case of a displaced oscillator model in this paper, the theory can be generalized to treat the cases of displaced–distorted oscillators, anharmonic effect, etc. It is hoped that with

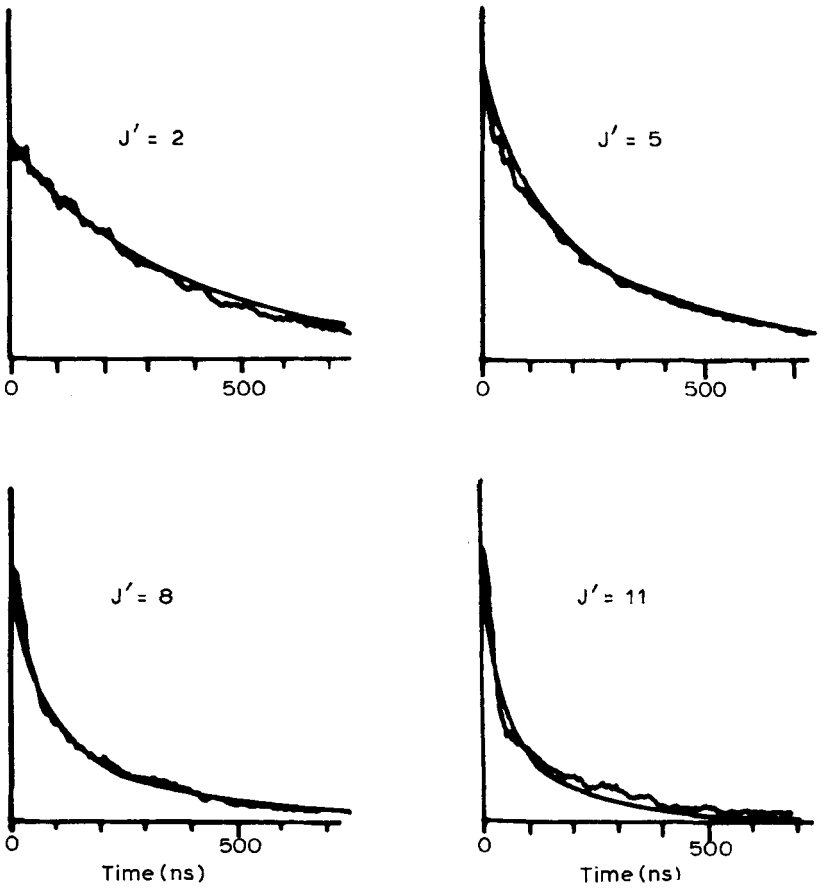

FIG. 33. Comparison between experimental and calculated time decays of pyrazine h_4. Experimental data are taken from Ter Horst *et al.* (1981). The smooth line is the theory.

the theoretical developments of Howard and Schlag, Novak and Rice and Henke *et al.* enough progress has been made that the theoretical method can now be used for analysing the experimental results of SRVL NR rate measurements.

From the discussion given in the experimental section, we can see that the radiative lifetimes can also exhibit the rotational effect. Although a similar treatment as that presented in the theory section can be applied to SRVL radiative processes, this has not been carried out. The SVL radiative process has been treated by Fleming *et al.* (1973).

Quantum beat

The quantum beat phenomenon represents a dramatic example of the superposition principle of quantum mechanics (or quantum interference). It has been observed with relative ease in atoms and diatomic molecules (Haroche, 1976; Wallenstein *et al.*, 1974), where the excited state level density is so sparse that it is readily possible to focus upon a pair of interfering levels. On the other hand, in large molecules, the excited state

level density can become very large so that it is virtually impossible not to coherently excite a superposition of a great number of excited levels, thereby washing out quantum beat phenomena. As mentioned in the previous section, intramolecular quantum beats in polyatomic molecules were first observed by Chaiken *et al.* (1979) by measuring the time-resolved fluorescence of biacetyl excited to single rovibronic states of the first excited singlet state.

To treat quantum beats theoretically, both the Schrödinger equation method (Jortner *et al.*, 1969; Villaeys and Freed, 1976; Rhodes, 1969, 1977; Grigolini and Lami, 1978; Delory and Tric, 1974; Zir and Rhodes, 1976) and the density matrix method (Miller, 1973; Lendi, 1980; Haberkorn *et al.*, 1980; Selzle *et al.*, 1981; Kono *et al.*, 1981) have been developed. Only the density matrix method will be discussed here. As discussed in the experimental section, the quantum beats of molecules exhibit pressure (or collision) dependence and are affected by magnetic fields. It has been shown that the statistical properties of the incident light reflect the time development of the excited states (Rhodes, 1969, 1971, 1980; Langhoff, 1977; Langhoff and Robinson, 1973a, 1973b, 1974; Berg *et al.*, 1974; Friedman and Hochstrasser, 1974; Tramer and Voltz, 1979); the coherent excitation is essential to understand the quantum beats in the fluorescence. In order to take into account these effects on quantum beats it is convenient to employ the density matrix method.

The starting point of the density matrix method is to consider an isolated system (or total system) which can be divided into a 'system of interest' (i.e., degrees of freedom of interest) and a 'reservoir' (i.e., irrelevant degrees of freedom) and to eliminate the irrelevant part of the density matrix to obtain the equation of motion for the reduced density matrix of the subsystem (or simply system) (Louisell, 1973; Lin and Eyring, 1977; Mukamel, 1979; Grigolini, 1981).

The time dependence of the density matrix of the total system (or isolated system) is determined by the Liouville equation of motion

$$\frac{d\hat{\rho}}{dt} = -\frac{i}{\hbar}(\hat{H}\hat{\rho} - \hat{\rho}\hat{H}) = -i\hat{L}\hat{\rho} \tag{56}$$

in which $\hat{L}$ represents the Liouville operator. The total system consists of a part called the system of interest with Hamiltonian $\hat{H}_s$ and of a reservoir with Hamiltonian $\hat{H}_b$. If we let $\hat{H}_1$ represent the interaction between the two parts, then the Hamiltonian of the total system can be written as

$$\hat{H} = \hat{H}_s + \hat{H}_b + \hat{H}_1 \tag{57}$$

In accordance with Eq. (76), the corresponding Liouville operator takes the form

$$\hat{L} = \hat{L}_s + \hat{L}_b + \hat{L}_1 \tag{58}$$

Notice that the density matrix of the system of interest at time t can be obtained by

$$\hat{\rho}^{(s)}_{(t)} = T_{r_b}[\rho(t)] \tag{59}$$

where T_{r_b} represents the operation of carrying out a trace over the quantum states of the reservoir. Many approaches have been developed to eliminate the reservoir variables to obtain the equation of motion for $\hat{\rho}^{(s)}(t)$; it can in general be expressed as

$$\frac{d\hat{\rho}^{(s)}}{dt} = -i\hat{L}_s\hat{\rho}^{(s)} - \int_0^t d\tau \langle \hat{M}_c(\tau)\rangle \rho^{(s)}(t-\tau) \tag{60}$$

where $\langle \hat{M}_c(\tau)\rangle$ is the memory kernel.

In the Markoff approximation, Eq. (60) reduces to

$$\frac{d\hat{\rho}^{(s)}}{dt} = -i\hat{L}_s\hat{\rho}^{(s)} - \hat{\Gamma}\hat{\rho}^{(s)} \tag{61}$$

where $\hat{\Gamma}$ is the so-called damping operator, and related to the memory kernel by

$$\hat{\Gamma} = \int_0^\infty d\tau \langle \hat{M}_c(\tau)\rangle \exp(i\tau\hat{L}_s) \tag{62}$$

The calculation of the matrix elements of $\hat{\Gamma}$ and the memory kernel has been well developed (Louisell, 1973; Ben-Reuven, 1975; Cukier and Deutch, 1969; Lin and Eyring, 1977; Mukamel, 1978).

Equations (60) and (61) can be used to treat relaxation processes. It should be noted that the diagonal matrix element $\rho_{nn}^{(s)}$ describes the population of the system, while the off-diagonal matrix element $\rho_{mn}^{(s)}$ describes the phase of the system and is closely related to the line-width and line-shape in optical spectra.

Using the isolated-line approximation (Baranger, 1958a,b; Yee and Gustafson, 1978), the matrix elements of Γ can be expressed as

$$\Gamma_{nn:nn} = -\sum_{m}^{m\neq n}{}' \Gamma_{mm:nn} \tag{63}$$

and

$$\Gamma_{mn:mn} = \tfrac{1}{2}(\Gamma_{mm:mm} + \Gamma_{nn:nn}) + \Gamma^{(d)}_{mn:mn} \tag{64}$$

where $-\Gamma_{mm:nn}$ represents the rate constant for the transition $n \to m$, $\Gamma_{nn:nn}$ the total decay rate constant, $\Gamma_{mn:mn}$ the dephasing rate constant and $\Gamma^{(d)}_{mn:mn}$ the so-called pure dephasing rate constant.

It should be noted that in finding the matrix elements for $\hat{\Gamma}$ we need the basis set for the system of interest. The choice of basis sets is determined by experiment. For this purpose, the Hamiltonian of the system of interest is often written as

$$\hat{H}_s = \hat{H}_s^0 + \hat{H}' \tag{65}$$

and one can choose the eigenfunctions of $\hat{H}_s^0$ or the eigenfunctions of $\hat{H}_s$ as a basis set (Mukamel, 1978).

Suppose we choose the eigenfunctions of H_s^0 as a basis set. Then the master equations in the isolated-line approximation can be obtained from Eq. (61) as (Haberkorn *et al.*, 1980)

$$\frac{d\rho_{nn}}{dt} = -\frac{i}{\hbar}\sum_{n'}(H'_{nn'}\rho_{n'n} - \rho_{nn'}H'_{n'n}) - \sum_{n'}\Gamma_{n'n'}\rho_{n'n} \tag{66}$$

and

$$\frac{d\rho_{mn}}{dt} = -(i\omega_{mn} + \Gamma_{mn})\rho_{mn} - \frac{i}{\hbar}\sum_{n'}(H'_{mn}\rho_{n'n} - \rho_{mn}H'_{n'n}) \tag{67}$$

Where for convenience we use the notations

$$\rho_{nn} \equiv \rho_{nn}^{(s)},\ \Gamma_{n:n'} = \Gamma_{nn:n'n'},\ \Gamma_{mn} = \Gamma_{mn:mn} \text{ etc.}$$

It should be noted that Kono *et al.* (1981) have used the molecular eigenstates as a basis set to study quantum beats.

In particular we consider the three-level system (or pseudo two-level system) with a representing the ground state and m and n denoting the states in which the quantum interference takes place. In this case we may assume that

$$H'_{an} = 0, \qquad H'_{am} = 0 \tag{68}$$

which means that there is no interaction of n and m with the ground state, respectively, and the master equations are given by

$$\frac{d\rho_{nn}}{dt} = -\frac{i}{\hbar}(H'_{nm}\rho_{mn} - \rho_{nm}H'_{mn}) - \Gamma_{n:n}\rho_{nn} - \Gamma_{n:m}\rho_{mm} \tag{69}$$

$$\frac{d\rho_{mm}}{dt} = -\frac{i}{\hbar}(H'_{mn}\rho_{nm} - \rho_{mn}H'_{nm}) - \Gamma_{m:m}\rho_{mm} - \Gamma_{m:n}\rho_{nn} \tag{70}$$

and

$$\frac{d\rho_{mn}}{dt} = -(i\omega_{mn'} + \Gamma_{mn})\rho_{mn} + \frac{i}{\hbar}H'_{mn}(\rho_{mm} - \rho_{nn}) \tag{71}$$

where $\omega_{mn'} = \omega_{mn} + (H'_{mm} - H_{nn'})/\hbar$. Here for simplicity, the excitation source has been assumed to be removed. For comparison, the Schrödinger equation approach for this model is given in the Appendix.

The above master equations can be applied not only to quantum beats, but also to steady state and time-resolved level anticrossing LAC (Lombardi *et al.*, 1980, 1981a,b; Haberkorn *et al.*, 1980), level crossing, double resonance, MOMRIE (Beyer and Kleinpoppen, 1978) etc. For example, to apply the master equation approach to LAC, we may choose $\hat{H}'$ to be due to the interaction of the molecule (or atom) with the applied external field. For the treatment of the time-resolved LAC, we have to solve the master equations given above; in this case, the quantum beat can usually be observed (Haberkorn *et al.*, 1980).

For the treatment of the conventional steady state LAC, we have to solve the master equations resulting from setting

$$\frac{d\rho_{nn}}{dt} = 0 \qquad \text{and} \qquad \frac{d\rho_{mn}}{dt} = 0 \tag{72}$$

The fluorescence intensity $I(t)$ of a dipole transition can be expressed in terms of $\hat{\rho}^{(s)}(t)$ as (Haroche, 1976; Kono *et al.*, 1981)

$$\begin{aligned} I(t) &= K\sum_f T_r[\hat{\rho}^{(s)}(t)\mu|f\rangle\langle f|\mu] \\ &= K\sum_f\sum_n |\mu_{nf}|^2\rho_{nn} + K\sum_f\sum_n\sum_{n'}{}^{n\neq n'}{}' \mu_{n'f}\cdot\mu_{fn}\rho_{nn'} \end{aligned} \tag{73}$$

where K represents the proportionality constant, μ is the dipole operator and f denotes the final states after emission. For example, let us apply Eq. (73) to the pseudo two-level system. In this case, Eq. (73) reduces to

$$I(t) = K(|\mu_{na}|^2\rho_{nn} + |\mu_{ma}|^2\rho_{mn}) + K(\mu_{na}\cdot\mu_{am}\rho_{mn} + \mu_{ma}\cdot\mu_{an}\rho_{nm}) \tag{74}$$

If $\mu_{ma} = 0$ (that is, only one of the excited state is dipole-allowed), then we obtain

$$I(t) = K|\mu_{na}|^2\rho_{nn}(t) \tag{75}$$

In this case, we only need $\rho_{nn}(t)$ to describe the quantum beat decay.

The analytical solution of the pseudo two-level problem can be carried out only when $\Gamma_{mn}^{(d)} = 0$ (i.e., the pure dephasing does not exist, and $\Gamma_{m:n} = \Gamma_{n:m} = 0$). This has been accomplished and applied to quantum beats (Lendi, 1980; Haberkorn *et al.*, 1980; Henke *et al.*, 1981) and time-resolved LAC (Haberkorn *et al.*, 1980). However, this solution is very complicated. For the purpose of the qualitative understanding of quantum beats and time-resolved LAC, we can make a further assumption $\Gamma_{m:m} = \Gamma_{n:n}$ (i.e., either the total decay rates are equal, or an average decay rate is introduced); in this case, we obtain

$$\frac{\rho_{nn}(t)}{\rho_{nn}(0)} = \frac{e^{-t\Gamma_{mn}}}{\Lambda_{mn}^2}\left[\left(\omega_{mn}'^2 + \frac{2}{\hbar^2}|H'_{mn}|^2\right) + \frac{2}{\hbar^2}|H'_{mn}|^2 \cos \Lambda_{mn} t\right] \tag{76}$$

where

$$\Lambda_{mn}^2 = \omega_{mn}'^2 + \frac{4}{\hbar^2}|H'_{mn}|^2.$$

Here for simplicity, it has been assumed that the system is initially populated at n.

From Eq. (76), we can see that the larger the energy gap ω'_{mn}, the less pronounced is the quantum beat and in the weak coupling limit $|H'_{mn}| \ll \omega'_{mn}$, the beat disappears. For $\omega'_{mn} = 0$ or the strong coupling limit $|H'_{mn}| \gg \omega'_{mn}$, one gets a complete modulation. Instead of dealing with the quantum beat decay curves, it is often convenient to analyse the corresponding Fourier spectra to obtain the physical constants, $\Gamma_{m:m}$, $\Gamma_{n:n}$, Γ_{mn}, ω'_{mn} and H'_{mn}. For this purpose, let us carry out the Fourier transformation of Eq. (76).

$$\bar{\rho}(\omega) = \int_{-\infty}^{\infty} dt e^{-it\omega} \frac{\rho_{nn}(t)}{\rho_{nn}(0)} = \frac{2\Gamma_{mn}}{\Lambda_{mn}^2}\left\{\frac{1}{\omega^2 + \Gamma_{mn}^2}\left(\omega_{mn}^2 + \frac{2}{\hbar^2}|H'_{mn}|^2\right) + \frac{|H'_{mn}|^2}{\hbar^2}\right.$$
$$\left.\left[\frac{1}{(\omega - \Lambda_{mn})^2 + \Gamma_{mn}^2} + \frac{1}{(\omega + \Lambda_{mn})^2 + \Gamma_{mn}^2}\right]\right\} \tag{77}$$

This indicates that the Fourier spectrum consists of the half-Lorentzian through the term $(\omega^2 + \Gamma_{mn}^2)^{-1}$ whose width is determined by Γ_{mn}, the dephasing constant, and the full-Lorentzian through the term $[(\omega - \Lambda_{mn})^2 + \Gamma_{mn}^2]^{-1}$ whose maximum position is determined by the beat frequency, and whose width is determined by Γ_{mn}. Other useful information will be the relative height of the two Lorentzian peaks, which is determined by

$$\left(\frac{\hbar^2 \omega_{mn}^2}{|H'_{mn}|^2} + 2\right)$$

The features of quantum beats discussed above are shown in *Figure 34*. The theory fits the experimental results quite satisfactorily. The master equations of many-level systems have been solved numerically for the case in which the pumping process can be described as a rate constant and for the case in which the pumping process is due to a classical radiation field (Selzle *et al.*, 1981; Haberkorn *et al.*, 1980). The physical constants of biacetyl determined by analysing the experimental data with the numerical solution of the master equations are presented in *Table 5*.

The collision (or pressure) effect on quantum beats has been observed. This effect can also be qualitatively understood by using Eq. (76). If $\rho_{nn}(t)_P$ represents $\rho_{nn}(t)$ at pressure P, then

$$\frac{\rho^{nn}(t)_P}{\rho_{nn}(t)_0} = \frac{\rho_{nn}(0)_P}{\rho_{nn}(0)_0} \exp\{-t[\Gamma_{mn}(P) - \Gamma_{mn}(0)]\} \tag{78}$$

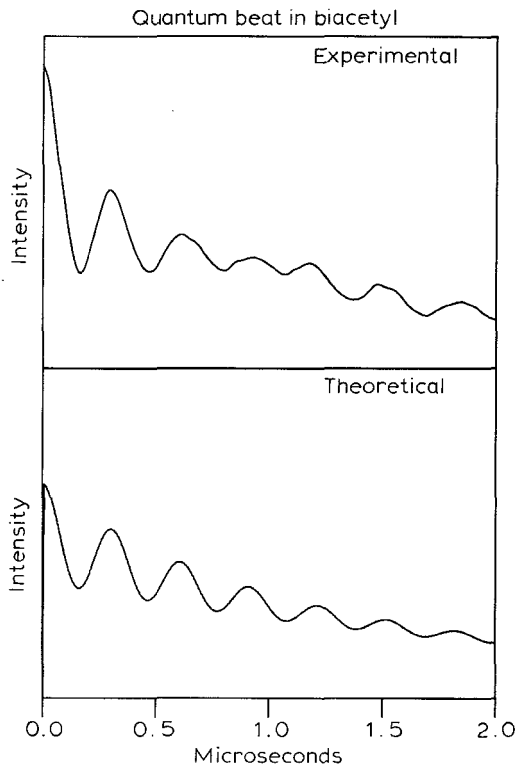

FIG. 34. Comparison between experimental and calculated quantum beat results. Experimental: 1_{01} rotational state in the 273 cm^{-1} excess energy vibrational state. Theoretical: input parameters of *Table 5* for zero magnetic field.

This indicates that the ratio of the two decay curves at two different pressures will approximately cancel the beat phenomenon and from the resulting exponential decay as a function of pressure, we can determine the collisional rate constant. This feature is observed experimentally and is shown in *Figure 24* (Chaiken *et al.*, 1981).

Henke *et al.* (1981) have observed the magnetic field effect on quantum beats in biacetyl. The experimental data have also been analysed by solving the master

TABLE 5. Quantum beat parameters in MHz for the 1_{01} rotational state of the 273 cm^{-1} excess energy vibrational state measured at 100 nozzle diameters and biacetyl seeded in 5 atm of He. The beat is displayed in *Figure 34*

	$H = 0$ G	$H = 4$ G
H'_{mn}	1.11	1.11
ω_{mn}	2.46	2.37
$\Gamma_{n:n}$	0.50	0.80
$\Gamma_{m:n}$	1.40	2.66

equations numerically and the quantum beat parameters obtained are presented in *Table 5*.

In concluding the discussion of this section, we would like to point out a number of theoretical problems which need to be solved, e.g. SRVL radiative rates, the effect of normal frequency displacement and anharmonicity on SRVL NR rates, vibration–rotation coupling in large amplitude vibrations, a better treatment of the effect of the Coriolis coupling on SRVL radiative and non-radiative rates, the magnetic field effect on photophysical processes of collision free molecules (Selzle *et al.*, 1979; Lin and Fujimura, 1979), etc.

ACKNOWLEDGEMENTS

The authors wish to thank DFG, the Alexander-von-Humboldt-Foundation and NSF US-Germany program for the financial support. One of us (S.H.L.) would like to thank Professor Hofacker for his hospitality.

APPENDIX

If we let u_n and u_m represent the eigenfunctions of $\hat{H}_s^0$ then in the Wigner–Weisskopf approximation for

$$\Psi(t) = c_n(t)u_n + c_m(t)u_m \tag{A-1}$$

we have

$$\frac{dc_n}{dt} = -(i\omega'_n + \tfrac{1}{2}\gamma_n)c_n - \frac{i}{\hbar}H'_{nm}c_m \tag{A-2}$$

and

$$\frac{dc_m}{dt} = -(i\omega'_m + \tfrac{1}{2}\gamma_m)c_m - \frac{i}{\hbar}H'_{mn}c_n \tag{A-3}$$

where γ_n and γ_m represent the total decay rates of the n and m states, respectively. γ_n and γ_m originate from the coupling of the system with the heat bath (e.g. radiation field, other irrelevant degrees of freedom etc).

Using the definition of the density matrix,

$$\rho_{nm}(t) = c_n(t)c_m^*(t); \qquad \rho_{nn}(t) = c_n(t)c_n^*(t) \tag{A-4}$$

and the time-dependent Schrödinger equation

$$(\hat{H}_s^0 + \hat{H}')\Psi(t) = i\hbar\frac{\partial\Psi}{\partial t} \tag{A-5}$$

we obtain

$$\frac{d\rho_{nn}}{dt} = -\frac{i}{\hbar}(H'_{nm}\rho_{mn} - \rho_{nm}H'_{mn}) - \gamma_n\rho_{nn} \tag{A-6}$$

$$\frac{d\rho_{mn}}{dt} = -\left(i\omega'_{mn} + \frac{\gamma_m + \gamma_n}{2}\right)\rho_{mn} + \frac{i}{\hbar}H'_{mn}(\rho_{mm} - \rho_{nn}) \tag{A-7}$$

etc. Equations.(A-6) and (A-7) should be compared with Eqs. (66) and (68); we can see that if we set $\Gamma_{n:m1=0\ and}\ \Gamma^{(d)}_{mn} = 0$, Eqs. (66) and (68) reduce to Eqs. (A-6) and (A-7), respectively. In other words, using the ordinary Schrödinger equation approach it is difficult to take into account the pure dephasing.

REFERENCES

AVOURIS, P., GELBART, W. M. and EL-SAYED, M. A. (1977). *Chem. Rev., 77*, 703.

BABA, H., FUJITA, M. and UCHIDA, K. (1980). *Chem. Phys. Letts., 73*, 425.

BARANGER, M. (1958a). *Phys. Rev., 111*, 481.

BARANGER, M. (1958b). *Phys. Rev., 111*, 494.

BARNETT, M., RAMSAY, D. A. and TILL, S. M. (1979). *Chem. Phys. Letts., 65*, 440.

BEN-REUVEN, A. (1975). *Adv. Chem. Phys., 33*, 235.

BERG, J. O., LANGHOFF, C. A. and ROBINSON, G. W. (1974). *Chem. Phys. Letts., 29*, 305.

BEYER, H. J. and KLEINPOPPEN, H. (1978). In: *Progress in Atomic Spectroscopy* (Eds. W. Hanle and W. Kleinpoppen), Part A, p. 607, New York: Plenum Press.

BIRSS, F. W., RAMSAY, D. A. and TILL, S. M. (1978). *Chem. Phys. Letts., 53*, 14.

BOESL, U., NEUSSER, H. J. and SCHLAG, E. W. (1975). *Chem. Phys. Letts., 31*, 1.

BRAND, J. C. D. and STEVENS, C. G. (1973). *J. Chem. Phys., 58*, 3331

BRAND, J. C. D. and LIU, D. S. (1974). *J. Chem. Phys., 78*, 2270.

BRUCAT, P. J. and ZARE, R. N. (1981). *28th IUPAC Congress*, Vancouver, Canada.

CHAIKEN, J., BENSON, T., GURNICK, M., and MCDONALD, J. D. (1979). *Chem. Phys. Letts., 61*, 195.

CHAIKEN, J., GURNICK, M. and MCDONALD, J. D. (1981). *J. Chem. Phys., 74*, 106.

CUKIER, R. I. and DEUTCH, J. M. (1969). *J. Chem. Phys., 50*, 36.

COVELESKIE, R. A. and PARMENTER, C. S. (1978). *J. Chem. Phys., 69*, 1044.

COVELESKIE, R. A., DOLSON, D. A., PARMENTER, C. S. and STONE, B. M. (1981). *J. Photochem., 1/2*, 165.

DELORY, J. M. and TRIC, C. (1974). *Chem. Phys., 3*, 54.

FAIRCHILD, P. W., GARLAND, N. L., HOWARD, W. E. and LEE, E. K. C. (1980). *J. Chem. Phys., 73*, 3046.

FISCHER, S. (1970). *J. Chem. Phys., 53*, 3195.

FLEMING, G. R., GIJZEMAN, O. L. J. and LIN, S. H. (1973). *Chem. Phys. Letts., 21*, 527.

FREED, K. F. (1976). *Topics Appl. Phys., 15*, 1.

FRIEDMAN, J. M. and HOCHSTRASSER, R. M. (1974). *Chem. Phys., 6*, 155.

GRIGOLINI, P. and LAMI, A. (1978). *Chem. Phys., 30*, 61.

GRIGOLINI, P. (1981). *Nuovo Cimento, 63B*, 174.

GURNICK, M., CHAIKEN, J., BENSON, T. and MCDONALD, J. D. (1981). *J. Chem. Phys., 74*, 99.

HABERKORN, R., SELZLE, H. L., DIETZ, W., LIN, S. H. and SCHLAG, E. W. (1980). *Chem. Phys., 52*, 363.

HALLIN, K. E. and MERER, A. J. (1977). *J. Mol. Spectrom., 65*, 163.

HAROCHE, S. (1976). In: *Topics in Applied Physics* (Ed. K. Shimoda), Vol. 13, p. 253, Berlin: Springer-Verlag.

HELLER, D. F., FREED, K. F. and GELBART, W. M. (1972). *J. Chem. Phys., 56*, 2309.

HENKE, W., SELZLE, H. L., HAYS, T. R. and SCHLAG, E. W. (1980). *Z. Naturforsch., 35a*, 1271

HENKE, W. E., SELZLE, H. L., HAYS, T. R., SCHLAG, E. W. and LIN, S. H. (1982a). *J. Chem. Phys., 76*, 1327.

HENKE, W. E., SELZLE, H. L., HAYS, T. R., SCHLAG, E. W. and LIN, S. H. (1982b). *J. Chem. Phys., 76*, 1335.

HENKE, W., SELZLE, H. L., HAYS, T. R., LIN, S. H. and SCHLAG, E. W. (1981c). *Chem. Phys. Letts., 77*, 448.

HENRY, B. R. and SIEBRAND, W. (1971). *J. Chem. Phys., 54*, 1072.

HENRY, B. R. and SIEBRAND, W. (1973). *Org. Mol. Photophys., 1*, 153.

HOWARD, W. E. and SCHLAG, E. W. (1976). *Chem. Phys., 17*, 123.

HOWARD. W. E. and SCHLAG, E. W. (1978a). *Chem. Phys.*, *29*, 1.
HOWARD, W. E. and SCHLAG, E. W. (1978b). *J. Chem. Phys.*, *68*, 2679.
HOWARD, W. E. and SCHLAG, E. W. (1980). In: *Radiationless Transitions* (Ed. S. H. Lin), p. 81, London: Academic Press.
INNES, K. K., KALANTAR, A. H., KHAN, A. Y. and DURNICK, T. J. (1972). *J. Mol. Spec.*, *43*, 477.
JOB, V. A., SETHURAMAN, V. and INNES, K. K. (1969). *J. Mol. Spec.*, *30*, 365.
JOUVET, C. and SOEP, B. (1980). *J. Chem. Phys.*, *73*, 4127.
JORTNER, J., RICE, S. A. and HOCHSTRASSER, R. M. (1969). *Adv. Photochem.*, *7*, 149.
KONO, H., FUJIMURA, Y. and LIN, S. H. (1981). *J. Chem. Phys.*, *75*, 2569.
KROTO, H. W. (1975). *Molecular Rotation Spectra*, Chichester: Wiley-Interscience.
KUSCH, P. and LOOMIS, F. W. (1939). *Phys. Rev.*, *55*, 850.
LANGHOFF, C. A. (1977). *Chem. Phys.*, *20*, 357.
LANGHOFF, C. A. and ROBINSON, G. W. (1973a). *Mol. Phys.*, *26*, 249.
LANGHOFF, C. A. and ROBINSON, G. W. (1973b). *Chem. Phys.*, *5*, 1.
LANGHOFF, C. A. and ROBINSON, G. W. (1974). *Chem. Phys.*, *6*, 34.
LEE, E. K. C. (1977). *Accts. Chem. Res.*, *10*, 319.
LEE, E. K. C. and LOPER, G. L. (1980). In: *Radiationless Transitions* (Ed. S. H. Lin), p. 1, London: Academic Press.
LENDI, K. (1980). *Chem. Phys.*, *46*, 179.
LIN, S. H. (1966). *J. Chem. Phys.*, *44*, 3759.
LIN, S. H. (1973). *J. Chem. Phys.*, *58*, 5760.
LIN, S. H. (1975). *J. Chem. Phys.*, *62*, 4500.
LIN, S. H. and EYRING, H. (1977). *Proc. Natl. Acad. Sci. USA*, *74*, 3623.
LIN, S. H. and FUJIMURA, Y. (1979). *Excited States*, *4*, 237.
LIN, S. H., WUTZ, D., HO, Z. Z. and EYRING, H. (1980). *Proc. Natl. Acad. Sci. USA*, *77*, 1245.
LOMBARDI, M., JOST, R., MICHEL, C. and TRAMER, A. (1980). *Chem. Phys.*, *46*, 273.
LOMBARDI, M., JOST, R., MICHEL, C. and TRAMER, A. (1981a). *Chem. Phys.*, *57*, 341.
LOMBARDI, M., JOST, R., MICHEL, C. and TRAMER, A. (1981b). *Chem. Phys.*, *57*, 355.
LOUISELL, W. H. (1973). *Quantum Statistical Properties of Radiation*, Chichester Wiley-Interscience.
LUNTZ, A. C. (1978). *J. Chem. Phys.*, *69*, 3436.
MICHEL, C. and TRAMER, A. (1979). *Chem. Phys.*, *42*, 315.
MILLER, T. A. (1973). *J. Chem. Phys.*, *58*, 2358.
MOULE, D. C. and RAO, C. N. R. (1973). *J. Mol. Spectry.*, *45*, 120.
MUKAMEL, S. (1979). *J. Chem. Phys.*, *71*, 2012.
MUKAMEL, S. (1978). *Chem. Phys.*, *31*, 327.
NOVAK, F. A. and RICE, S. A. (1979). *J. Chem. Phys.*, *71*, 4680.
NOVAK, F. A. and RICE, S. A. (1980). *J. Chem. Phys.*, *73*, 858.
NOVAK, F. A., RICE, S. A., MORSE, M. A. and FREED, K. F. (1980). In: *Radiationless Transitions*, (Ed. S. H. Lin), p. 135, London: Academic Press.
OHTA, N. and BABA, H. (1981). *Chem. Phys. Letts.*, *84*, 308.
PARKIN, J. E., POOLE, H. G. and RAYNES, W. T. (1962). *Proc. Chem. Soc. London*, 248.
PARMENTER, C. S. and RORDORF, B. F. (1978). *Chem. Phys.*, *27*, 1.
PARMENTER, C. S. and SCHUH, M. D. (1972). *Chem. Phys. Letts.*, *13*, 120.
RAMSAY, D. A. and TILL, S. M. (1979). *J. Can. Phys.*, *57*, 1224.
ROBINSON, G. W. and FROSCH, R. P. (1962). *J. Chem. Phys.*, *37*, 1962.
RHODES, W. (1969). *J. Chem. Phys.*, *50*, 2885.
RHODES, W. (1971). *Chem. Phys. Letts.*, *11*, 179.
RHODES, W. (1977). *Chem. Phys.*, *22*, 95.
RHODES, W. (1980). In: *Radiationless Transitions*, (Ed. S. H. Lin), p. 219, London: Academic Press.
ROBINSON, G. W. (1974). *Excited States*, *1*, 1.
SCHLAG, E. W., SCHNEIDER, S. and FISCHER, S. F. (1971). *Ann. Rev. Phys. Chem.*, *22*, 405.
SHARFIN, W., IVANCO, M. and WALLACE, S. C. (1981). *28th IUPAC Congress*, Vancouver, Canada.
SELZLE, H. L. and SCHLAG, E. W. (1979). *Chem. Phys.*, *43*, 111.

SELZLE, H. L., DIETZ, W., HABERKORN, R., LIN, S. H. and SCHLAG, E. W. (1981). *Nuovo Cimento, 63B*, 420; Paper presented at the *European Conference on the Dynamics of Excited States* held in Pisa, 14–16 April, 1980.
SETHURAMAN, V., JOB, V. A. and INNES, K. K. (1970). *J. Mol. Spec., 33*, 189.
SHIBUYA, K., FAIRCHILD, P. W. and LEE, E. K. C. (1981). (Submitted to *J. Chem. Phys.*).
STREK, W. (1978). *Chem. Phys. Letts., 57*, 121.
TANAKA, K., YAMADA, K., NAKAGAWA, T. and KUCHITSU, K. (1975). *J. Mol. Spec., 54*, 243.
TANG, K. Y., FAIRCHILD, P. W. and LEE, E. K. C. (1977). *J. Chem. Phys., 66*, 3303.
TER HORST, G., PRATT, D. W. and KOMMANDEUR, J. (1981). *J. Chem. Phys., 74*, 3616.
TRAMER, A. and VOLTZ, T. (1979). *Excited States, 4*, 281.
VILLAEYS, A. and FREED, K. F. (1976). *Chem. Phys., 13*, 271.
WALLENSTEIN, R., PAISNER, J. A. and SCHAWLOW, A. L. (1974). *Phys. Rev. Letts., 33*, 1063.
WEISSHAAR, J. C. and MOORE, C. B. (1979). *J. Chem. Phys., 70*, 5135.
WEISSHAAR, J. C. and MOORE, C. B. (1980). *J. Chem. Phys., 72*, 5415.
YEE, T. K. and GUSTAFSON, T. K. (1978). *Phys. Rev., 18A*, 1597.
ZIV. A. and RHODES, W. (1976). *J. Chem. Phys., 65*, 4895.

NOTE ADDED IN PROOF

Lambert *et al.* (1981) published quantum beats in anthracene after submission of this manuscript. These beats very likely are caused by interference of two singlet levels and thus more resemble those known from atoms or diatomics

LAMBERT, W. R., FELKER, P. M. and ZEWAIL, A. M. (1981). *J. Chem. Phys., 75*, 5958.